SURFACE MODIFICATION OF TITANIUM ALLOY FOR BIOCOMPATIBILITY

Salikh Omarov, B.Eng. in Mechanical Engineering

Submitted in fulfillment of the requirements
for the degree of Master of Science
in Mechanical & Aerospace Engineering

NAZARBAYEV UNIVERSITY

School of Engineering and Digital Sciences
Department of Mechanical & Aerospace Engineering
Nazarbayev University

53 Kabanbay Batyr Avenue,
Astana city, Kazakhstan, 010000

Supervisor: Assistant Professor Asma Perveen
Co-supervisor: Associate Professor Didier Talamona

April 2023

DECLARATION

I hereby, declare that this manuscript, entitled "*surface modification of titanium alloy for biocompatibility*", is the result of my own work except for quotations and citations, which have been duly acknowledged.

I also declare that, to the best of my knowledge and belief, it has not been previously or concurrently submitted, in whole or in part, for any other degree or diploma at Nazarbayev University or any other national or intentional institution.

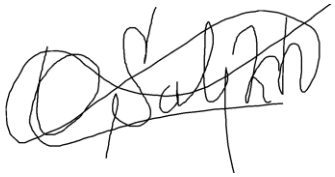

Name: Salikh Omarov

Date: 7.4.2023

Abstract

Despite the research development in biomedicine, orthopedical implant application is still facing several challenges. The relatively vast number of implant failures in long-term applications motivates the current research to reduce their possibilities to occur. One of the vital aspects in achieving that is modification of implant surfaces. So far, many surface modification techniques have been investigated, however, electro discharge machining (EDM) is a promising technique in surface treatment of conductive materials such as titanium alloys. Moreover, printing implants with selective laser melting (SLM) is gaining bigger attention due to the flexibility of production of complex bone-like shapes. The thesis work is focused on modification of mechanical properties as well as biocompatibility of machined surfaces of both casted and printed biomedical Ti-6Al-4V titanium alloys by EDM through altering surface characteristics. Machining performance such as material removal rate (MRR), overcut and kerf width and surface aspects such as surface roughness, crater sizes, hardness, surface free energy and biofilm formation of pseudomonas aeruginosa bacteria are observed. Based on these results, the effects of parameter values of gap voltage, pulse current, time on and duty factor of drilling EDM as well as parameter values of capacitance and voltage of micro EDM were observed. Comparing casted and printed titanium alloys, modifications of surfaces on printed titanium alloy have better performance in MRR, kerf width, crater size and surface roughness, meanwhile, casted titanium alloy has better performance in contact angle and hardness values. Moreover, despite high overall resistance on bacteria adhesion and biofilm formation, biological analysis showed that these results correlate with discharge energy of EDM process. Low discharge energy resulted in a bigger number of bacterial strains while high energy had better resistance to bacteria. Therefore, by analyzing the effect of EDM on modified surface, it was observed that the resistance to bacteria adhesion and biofilm formation increased for higher discharge energy while comparison between casted and printed titanium alloy showed that printed titanium alloy has better performance in EDM treatment for biocompatibility purposes.

Keywords: Electro discharge machining, titanium alloys, biomedical implant material, selective laser melting, Ti-6Al-4V, biofilm formation, bacteria adhesion

Acknowledgements

I would like to express my deepest gratitude to the following people who have helped and supported me throughout the completion of this thesis: First and foremost, I would like to thank my thesis supervisor professor Asma Perveen and co-survivor Didier Talamona, for providing me with invaluable guidance, encouragement, and feedback throughout the research process. Your expertise, knowledge, and patience have been instrumental in shaping this thesis and helping me achieve my academic goals. I would like to thank professor Tri Pham, Ainur Kenessova and Faisal Nazir for their assistance and contribution in the biological side of the thesis. I, also, would like to thank my family, friends, and colleagues who have supported me throughout my academic journey. Your words of encouragement, emotional support, and understanding have been a source of strength and motivation for me. Thank you all for your support and encouragement.

Table of Contents

List of Abbreviations & Symbols

BCC	Body Center Cubic
EDM	Electro Discharge Machining
SLM	Selective Laser Melting
MRR	Material Removal Rate
TWR	Tool Wear Rate
TW	Tool Wear
OC	Overcut
SR	Surface Roughness
SEM	Scanning Electron Microscope
EDX	Energy-Dispersive X-Ray Spectrograph
CAD	Computer Aided Design
GRA	Grey Relation Analysis
SB	Smaller-Is-Better
LB	Larger-Is-Better
OD	Optical Density
D	Diameter of Machined Hole at Entrance
d	Smaller Diameter of Machined Hole at Exit
h	Depth of Machined Hole
t	Machining Time
I_w	Working Current
I_p	Pulse Current
T_{on}	Time-on
T_{off}	Time-off
V_g	Gap Voltage

List of Tables

List of Figures

Chapter 1 – Introduction

1.1. Background

Titanium and its alloys are novel materials that are recently studied in order to be implemented in orthopedical biomedicine. In fact, compared to its predecessors, these materials obtain better performance in terms of biocompatibility [1]. However, the current direction of the research is focused on performing surface treatment that can enhance their performance in the human body environment. Currently, there are several biocompatibility issues that can be improved by proper surface treatment techniques of biomedical materials. First of them is the mechanical properties of the surface. Due to the highly inert environment of the human body as well as continuous and cyclic loading on an implant by adjacent tissue, the surface of the implant can be damaged forming debris of metal ions that can be released into the human body or, moreover, lead to implant failure. Second, appropriate topography is another vital requirement. This parameter is responsible for cell attachment which further results in tissue ingrowth into materials [2]. This type of issue can be addressed by using electro-discharge machining (EDM). In fact, this machining technique is capable of forming surface topology in micro-scales which is important for attachment of human cells [3].

1.2. Problem Statement and Motivation

Titanium and its alloys have been extensively studied for their potential use in orthopedic applications due to their favorable mechanical and biocompatible properties. Despite these advantages, the inert nature of the implant surface and continuous loading by adjacent tissues can lead to damage, metal ion debris, and ultimately implant failure. In addition, inappropriate surface topography can prevent cell attachment and inhibit tissue growth, which can limit the implant's effectiveness.

Currently, there are various surface treatments and machining techniques that have been developed to improve the surface properties of biomedical materials. However, there is a lack of research that has directly compared the effectiveness of these techniques on cast and 3D-printed titanium alloys. Therefore, there is a need to investigate the effectiveness of different surface treatments and machining techniques on cast and 3D-printed titanium alloys for use in orthopedic applications.

The motivation for this study is to investigate an effective surface treatment method and machining technique for titanium and its alloys in micro scale with EDM, which will improve their performance as orthopedic implants. The study aims to investigate the effectiveness of different surface treatment and machining parameters on both cast and 3D-printed Ti-6Al-4V, with a focus on their mechanical and biocompatible properties.

By comparing the surface properties and biocompatibility of the treated and untreated surfaces of cast and 3D-printed titanium alloys, this study can provide insights into the most effective surface treatment and machining technique for use in orthopedic implants. This research can potentially lead to the development of a novel surface treatment technique that enhances the mechanical and biocompatible properties of titanium alloys which in turn improves their long-term effectiveness as orthopedic implants.

1.3. Research Aims and Objectives

The aim of the research is to investigate the possibilities of EDM technique to improve biocompatibility of implant material under different machining parameters. There are several objectives established to complete the aim of the project:

i. To study the machinable parameters of different EDM machines for Ti-6Al-4V alloy;
ii. To investigate the difference of machining performance on casted and 3D printed Ti-6Al-4V alloy;
iii. To evaluate surface morphology properties of the formed surfaces;
iv. To investigate the capability to prevent bacterial adhesion of the formed surface by biofilm formation and investigate the relations with topographic and mechanical results.

Chapter 2 – Literature Review

2.1. Introduction

This chapter is dedicated to the literature review on the topic and presents a review of the past work in order to gain some background knowledge on basic understandings. Moreover, it provides several studies about what was investigated and done so far by other authors in two main fields. These fields are biomedical titanium alloys and surface treatment with electro discharge machining. Also, the conjunction of both areas is reviewed. Firstly, Section 2.2, provides descriptive information about biomedical materials. In detail, the types of biomedical materials, their application, advantages and disadvantages of each metallic alloys and more in-depth information about titanium alloys in orthopedical applications. Section 2.3 is about EDM and its basic understanding of its operation. Lastly, section 2.4 presents some experimental studies on the crossing area of research.

2.2. Biomedical materials

There are different types of materials used in biomedicine for implant purposes. Due to the complexity of the human body, each of its parts require specific classification of implants in order to be biocompatible as well as appropriately functional in terms of physical behavior in applications such as stents in blood vessels, artificial valves in hearts, replacement of bones, and etc. Based on that, biomaterials are separated into four material groups [4] which are:

- Metallic
- Ceramic
- Polymeric
- Composite

Furthermore, different types of material are better to implement in different parts of the human body. As a couple of examples, cobalt alloys are good in replacement of full joints, magnesium (Mg) is good in application of biodegradable implants in orthopedic and so on [4]. However, the focus of the research is aimed on Metallic materials based on titanium (Ti) alloys. Metallic materials are widely used as bone fixation tools and complete bone replacing implants [5]. Ti was found to be the most biocompatible material among other metallic materials in this area of application [6]. The reasons for that are due to the following advantages:

- Good bioactivity – slow growth of titanium hydrated oxide layer results in important reactions with calcium (Ca) and phosphorus (P) in the human body.
- High corrosion resistance – Ti and its alloys have the unique feature of forming an extremely stable oxide layer on the top of the surface resisting chemical corrosions with water, salts or acids.
- Satisfactory mechanical properties – Ti and its alloys have high tensile strength with a combination of low elastic modulus which is close to the properties of bone compared to other materials [5].

Nevertheless, currently, there is no perfect solution for implant material which matches all criteria of biocompatibility. From worldwide practice, Ti-6Al-4V was found to be the most satisfactory material for implant application. However, the latest studies estimated that vanadium (V) has an abnormal amount of toxicity effect on the human body [5]. This problem requires either alternative material or surface treatment techniques to reduce unwilling effects on the human body. Biocompatibility of Ti alloys are characterized by three main parameters which are toxicity, carcinogenicity and metal sensitivity. Also, the material should be bio-tolerant, bioactive and bioinert which represent the behavior of bone ingrowth into material in indirect contact, direct contact and its bonding, respectively [4, 7].

Corrosion resistance of the implant material is also an important parameter to consider. Many studies have been paying extra attention to it due to its importance in terms of biocompatibility. This is due to the highly active environment of the body which causes corrosive reactions of the metals affecting its durability or even leading to implant failures. Moreover, release of ions takes place due to unsatisfied corrosion resistance which is possible to cause cancer or hypersensitivity. Other than that, corrosion of the implant can be emphasized in combination with external loads and wear [8]. As it was stated, the ability of titanium alloy to quickly form a titanium oxide layer is a big advantage over currently used stainless steel and cobalt-chromium alloys. However, this aspect still requires improvements to increase its durability. In the study of [9], the corrosion resistance of Ti-6Al-4V was increased by 96.63% by using powder mixed-EDM.

2.3. Electro discharge machining (EDM)

Despite studying the proper material for biomedical implants, their surface performances are vital as well. In fact, there are many surface treatment techniques, however, EDM treatment is one of the most versatile surface treatment techniques which can affect biocompatibility aspects of the material surface of implants. Its non-contact approach of surface treatment, which is based on electrical sparks between tool electrode and conductive workpiece (see Figure 2.1), allows high-precision machining which is required for multi-scale surface forming of implants. By transferring electrical energy into thermal energy, the spark is created by applying a high voltage across the gap between the tool and workpiece, which ionizes the dielectric fluid and creates a conductive plasma channel. When the plasma channel is formed, the temperature within the channel rises rapidly, reaching up to 20,000 ℃. This high temperature causes the workpiece material to vaporize and melt, which is then removed by the dielectric fluid flow. As the EDM process continues, the spark discharges repeatedly at a high frequency, resulting in the progressive erosion of the workpiece material [10]. The surface treatment properties of EDM mainly depend on discharge energy and the duration of the energy, however, there are several parameters such as peak current, gap voltage, time-on and time-off that are optimized depending on the aim of the surface treatment technique. While peak current and gap voltage contribute to the amount of discharge energy, time-on and time-off defines the duration of sparks and idle time between sparks, respectively [11]. These factors can have some effects on osteointegration as well as mechanical properties of the implant.

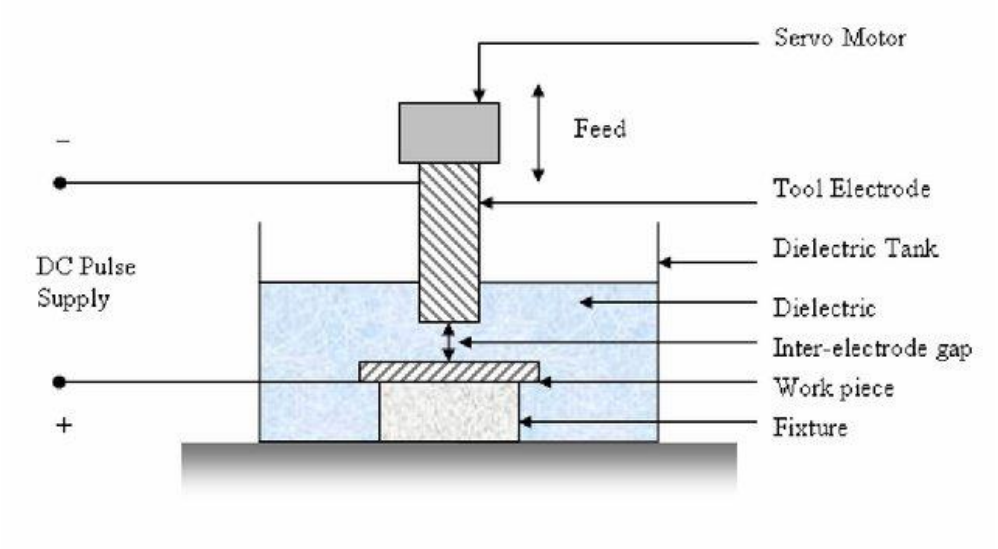

Figure 2.1: Schematic of EDM process [12]

There are several types of EDM techniques such as drilling EDM, die-sinking EDM, and wire EDM that can perform surface treatment in different approaches. By utilizing EDM in industrial needs, wire-EDM (WEDM) became the most favorable surface treatment technique among them in most applications. This type of machining uses a thin wire as an electrode which is supplied continuously and can travel as well as machine in a more free manner as shown in Figure 2.2 compared to other mentioned techniques. It is very useful to machine hard-to-cut materials in the required shape, reducing the need for preparing electrode tools common in other EDM techniques [10].

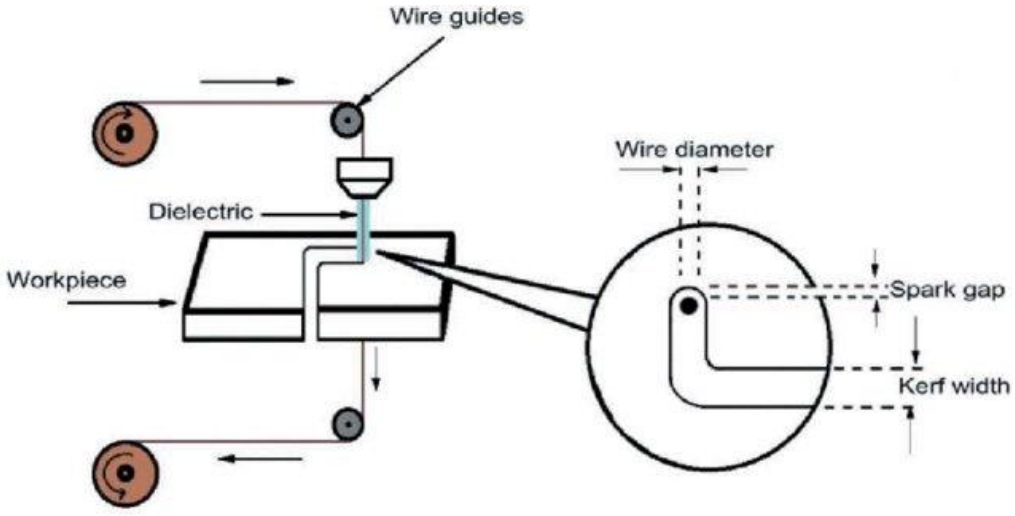

Figure 2.2: Schematic of wire EDM process [13]

2.4. Selective laser melting

One of the scopes of the paper is to compare EDM machining on titanium plates printed by using selective laser melting (SLM). SLM is the additive manufacturing process which allows to manufacture three-dimensional (3D) objects. It implies a high power-density laser beam on selective areas of powder in order to melt as well as fuse them to form a solid layer, repeating the procedure for each layer step by step producing a 3D model of an object according to computer aided design (CAD). This approach of manufacturing allows to fabricate components with complex shapes which would be challenging to produce by using traditional manufacturing methods. In the field of biomedicine, this technology is very useful due to the demand of complex shaped and individual implant fabrication. These custom matched implants allow to reduce the number of revision surgeries [14].

The combination of SLM and EDM in manufacturing of biomedical implants can enhance the quality of products. While SLM can produce parts with specific needs in terms of geometries, EDM can modify the surface properties of SLM printed parts. By considering various factors such as design, material and optimized process parameters, involving both techniques can result in enhanced quality implants with improved biocompatibility, mechanical properties and precisely controlled surface properties [15].

2.5. Experimental studies

There are several experimental studies that performed EDM machining on titanium alloys in order to investigate the differences in mechanical characteristics between untreated and treated surfaces of workpieces. In the study of [16], Ti-6Al-4V was machined by using micro-EDM drilling technique. They investigated the effects of changing parameters such as peak current, pressure of flushing dielectric, pulse-on-time and duty ratio on the output parameters such as material removal rate (MRR), tool wear rate (TWR), taper angle and overcut (OC). They observed that time-on parameter has the biggest effect on MRR, taper and OC, while peak current contributes TWR the most. The values of MRR and TWR change in tandem with discharge energy which is controlled by peak current values, however, time-on tends to have lower MRR at its low and high values. Meanwhile, duty factor and flushing pressure have the least effect on MRR and TWR. In terms of OC and taper angle, these parameters change proportionally to the values of

peak current and time-on. Lastly, the sizes of recast layers are decreased for lower values of time-on and peak current. [3] stated that titanium alloys treated with EDM techniques increase surface hardness, wear and corrosion resistance. However, fatigue performances of the machined surfaces become less. Despite that, the possibility to form carbide and oxide layers on the surface with controlled thickness increases the biocompatibility of the machined material surfaces.

As well, several studies were done in order to investigate the effect on biocompatibility of EDM treatment on Ti-6Al-4V alloys. In the study of [17], EDM modification of Ti-6Al-4V surfaces was done. In the study, it was observed that formation of TiO_2 thin layer enhanced cell compatibility. Also, increased time-on values enhance the activity of osteoblast cells. Another study [18], observed that micro EDM technique is capable of producing surfaces with roughness lower than 100 μm which is vital for biocompatibility. Moreover, the authors observed that the porous layer of TiO_2 allows to increase morphological fixation of bone with implant surface. In addition, microhardness of the surface was increased which can reduce the wear hence emitting implant ions to the human body. Regarding resistance to biofilm formation and bacteria adhesion, current research is focused on powder mixed-EDM (PW-EDM) where matching powder compositions for reducing bacterial activity are selected. However, to my extent, there are not many studies focused on correlation between classical EDM process and resistance to bacterial adhesion and biofilm formation.

Chapter 3 – Methodology

3.1. Introduction

Surface treatments of titanium alloy are performed on different types of EDM machines which are drilling EDM and micro EDM. Micro EDM was done by using micro drilling EDM and micro wire EDM techniques. This will allow it to perform a surface treatment process in both macro and micro scale. In order to minimize the number of experiments Taguchi's orthogonal arrays are implemented. The experiments on drilling EDM are focused on making circular blind holes as shown in Figure 3.1, while machining by using micro wire EDM allows to obtain machined areas of surfaces. The experiments are performed on Ti-6Al-4V. Section 3.2 is dedicated to the material the paper is focused on. While sections 3.3 and 3.4 were written about the experimental set-up. Lastly, section 3.5 is about taking measurements and collecting the results from produced experiments.

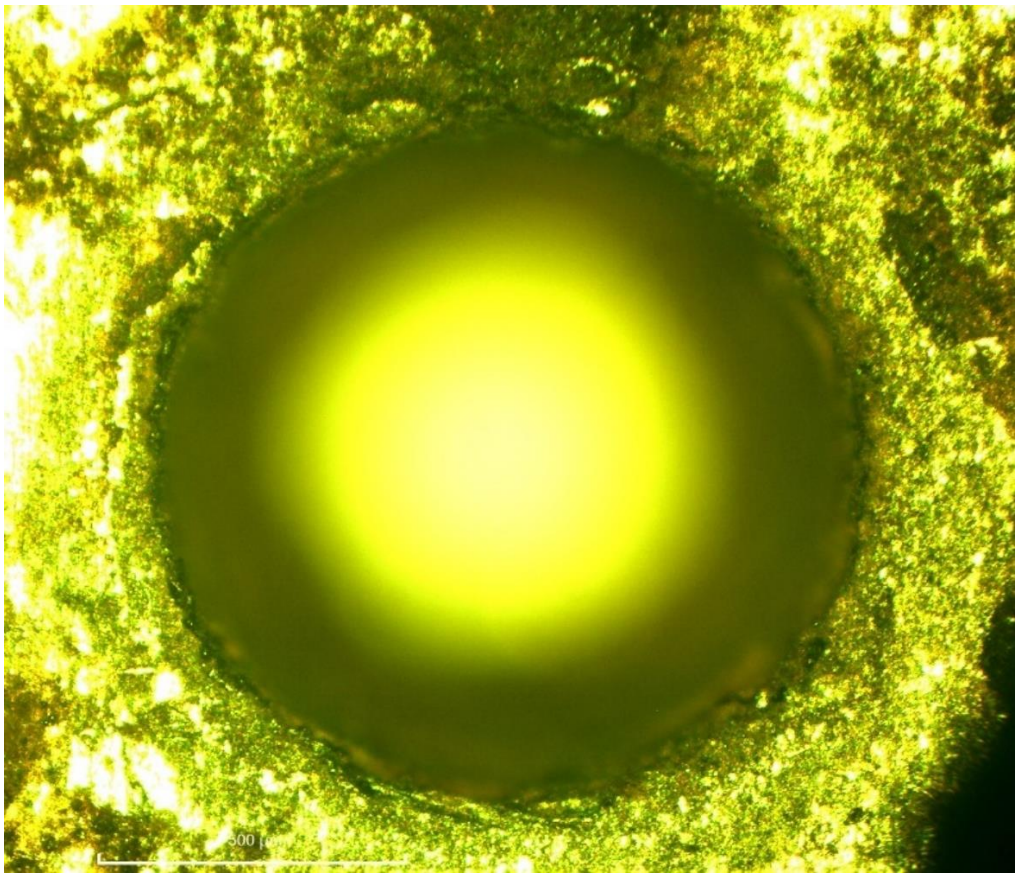

Figure 3.1: Microscopic photo of a through hole machined by drilling EDM

3.2. Material

The machined workpieces are Ti-6Al-4V titanium alloy plates. This type of alloy has advantages over currently used implant biomaterials such as low density and excellent corrosion resistance. For these reasons, the mentioned alloy has gained interest among its class in orthopedic applications. This alloy is divided into two types in terms of production. First of them are titanium alloys. Second are 3D printed with SLM process. The workpiece dimensions were 20 mm × 20 mm × 3 mm plate and their compositions are shown in Table 3.1. Moreover, EDX results are shown in Figure 3.2.

Table 3.1: Chemical composition of workpiece

Element	Al	V	Ti
wt%	6	4	Balance

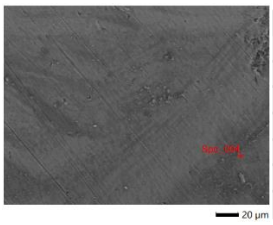

Element	Line	Mass%	Atom%
C	K	5.23±0.04	17.34±0.12
Na	K	0.13±0.02	0.22±0.03
Al	K	5.96±0.05	8.80±0.07
Ti	K	85.78±0.18	71.36±0.15
V	K	2.91±0.05	2.28±0.04
Total		100.00	100.00
Spc_004			Fitting ratio 0.0061

Figure 3.2: EDX analysis of casted workpiece

3.3. Drilling EDM

The experiments on macro scale were performed using DD703.30A drilling EDM machine produced by BOFENG Machinery. The experimental methods and conditions of machining blind holes on the alloy as well as approach on measuring the results are presented in the following subsections.

3.3.1. Machining Parameters

The study is focused on investigating the effects of machining parameters such as time-on, time-off, peak current and gap voltage. The results are evaluated based on the effects of material removal rate (MRR) and overcut (OC). During the experiments, feed rate, spindle rotation speed and flushing pressure were constant. The unitless values of the parameters represent the input parameters defined by the machine. These values of machining parameters are defined between 1 and 10 where 1 is the lowest value and 10 is the highest value for a parameter. Feed rate was set to value 4 and flushing pressure was set to 10 MPa. Table 3.3 shows different values of machining parameters affecting machining properties. The

experimental design was established by using Taguchi's L9(3^4), an orthogonal array with four parameters and three levels. As a result, the number of required experiments was dropped to nine in order to evaluate the effect of each parameter. The set is shown in

Table 3.4. Working current (Iw) was also changed in tandem with peak current (Ip) in order to maintain proper feedback sensitivity. The experiments were conducted three times so that the average values of measurements could be collected. The electrode was pure brass hollow tube with outer and inner diameters of 1 mm and 0.4 mm, respectively. Its physical properties are shown in Table 3.2. The dielectric fluid was distilled water. Figure 3.3 shows the machined holes by drilling EDM.

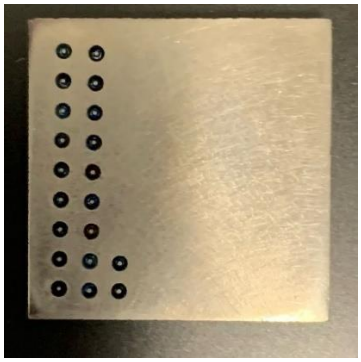

Figure 3.3: Top view on titanium plate for drilling EDM.

Table 3.2: Physical properties of brass electrode

	Density (g/cm3)	**Melting temperature (℃)**	**Thermal conductivity (W/m.k.)**
Brass	4.43	1650	7.2

Table 3.3: Machining Parameters

Parameter	**Symbol**		**Levels**			**Unit**
			1	*2*	*3*	
Peak current	I_p	A	2	5	8	
Working current	I_w		2	5	8	
Time-on	T_{on}	B	2	5	8	
Time-off	T_{off}	C	2	5	8	
Gap	V_g	D	2	5	8	
Fixed parameters						
Flushing pressure	P_f		5			MPa
Machining depth	H		1			mm
Servo speed	V_s		4			
High volts	HV		2			

Table 3.4: Experimental set based on Taguchi's orthogonal array

Exp. No.	I_p/ I_w	T_{on}	T_{off}	V_g
1	2	2	2	2
2	2	5	5	5
3	2	8	8	8
4	5	2	5	8
5	5	5	8	2
6	5	8	2	5
7	8	2	8	5
8	8	5	2	8
9	8	8	5	2

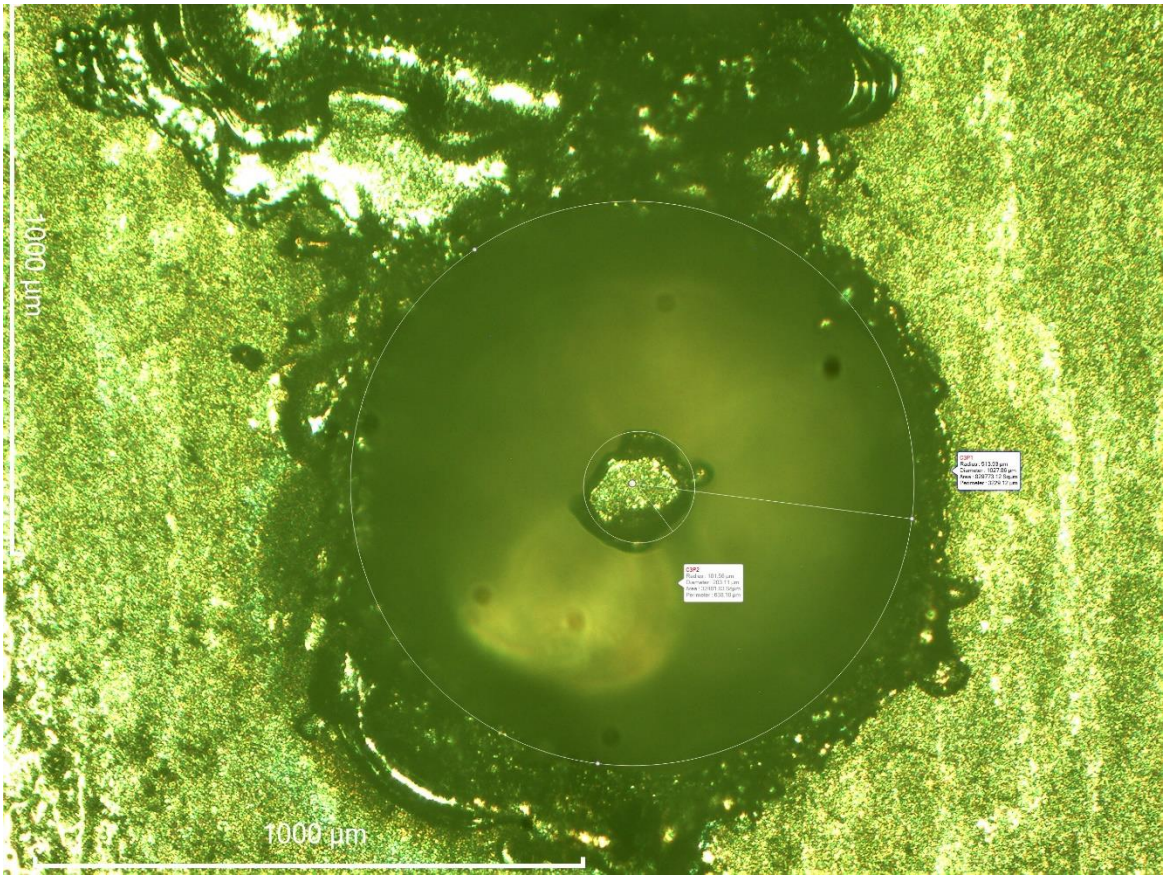

Figure 3.4: Surface profile is a blind hole after machining 1 mm blind hole

The machining properties are evaluated in terms of MRR and OC. MRR was calculated with volumetric loss over machining time. The volume loss is calculated by multiplying the machined area by the depth of the blind hole. Figure 3.4 depicts the surface profile of the machined area. Due to the hollow shape of the electrode, the workpiece is machined incompletely, and thus the area of the untreated surface is subtracted. The difference between the inner and outer diameters

of the hole and the inner and outer diameters of the tool was used to calculate the overcut. For that purpose, three dot circles were used to estimate each diameter. In total, the mean value from four measurements was calculated. The following formulas were used to calculate MRR and overcut:

$$MRR = \frac{\textbf{Volumetric loss of the material during machining } (mm^3)}{\textbf{Machining time } (min)} = \frac{\left(\textbf{Area of the hole } (mm^2) - \textbf{Untreated area } (mm^2)\right) * \textbf{Depth } (mm)}{\textbf{Machining time } (min)} \quad (1)$$

$$OC_{outer} = \frac{\textbf{Hole diameter} - \textbf{Tool diameter}}{2} \quad (2)$$

$$OC_{inner} = \frac{\textbf{Tool inner diameter} - \textbf{Diameter of untreated surface}}{2} \quad (3)$$

$$OC = \frac{OC_{outer} + OC_{inner}}{2} \quad (4)$$

In the analysis of Taguchi's method, MRR and overcut are categorized as "higher-is-better" and "lower-is-better", respectively. These results are also normalized for grey relation analysis (GRA) and by using GRA and ANOVA, the optimum combinations of parameters are predicted.

3.3.2. Software and Equipment

In order to measure the diameters of the holes, an optical microscope was used in tandem with Motic Images Plus 3.1 software. The machining time was calculated by using a 240 frame-per-seconds slow motion camera. Minitab 19 software was used for analytical estimations.

3.4. Micro EDM

The machining of Ti-6Al-4V alloy plates in micro scale was done by using a DT110i hybrid micro-EDM machine by Mikrotools. There are two types of EDM techniques implemented in the study of micro EDM which are micro drilling EDM and micro wire EDM.

3.4.1. Micro drilling EDM

The experimental set for micro drilling EDM is based on Taguchi's orthogonal array with a smaller number of parameters since the machine is based on a resistor-capacitor circuit. Taguchi's L9(3^3) orthogonal array consists of factors which are voltage, capacitance and spindle speed. These parameters have three levels as shown in Table 3.5. As for experiments for drilling EDM, a set consists of 9 experiments, which are repeated 3 times for post experimental analyses

of estimating mean measurement for MRR, and OC. The total number of experiments is 27. Several machined micro holes are shown in Figure 3.5

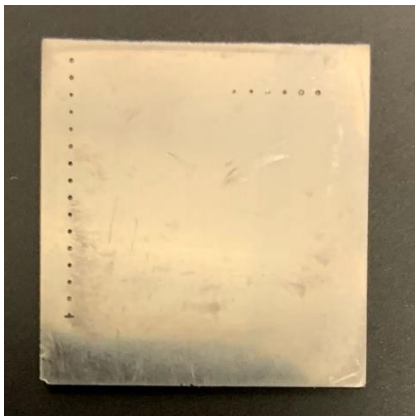

Figure 3.5: Top view on titanium plate for micro drilling EDM

The parameters such as electrode tool spindle speed, feed rate, electrode material (tungsten carbide) and dielectric fluid (deionized water) are the same for each experiment. In detail the tungsten carbide tool electrode diameter was 260 μm and depth of cut of 150 μm. The feed rate was equal to 0.06 mm/min as an optimal feed rate for all experimental parameters, however, actual feed rate is decreased from feedback system control.

Table 3.5: Taguchi's orthogonal array for micro drilling EDM

#	Voltage, V	Capacitance, pF	Spindle speed, rpm
1	90	1	750
2	90	10	1000
3	90	100	1250
4	100	1	1000
5	100	10	1250
6	100	100	750
7	110	1	1250
8	110	10	750
9	110	100	1000

3.4.2. Micro wire EDM

Meanwhile, micro wire EDM was based on Taguchi's orthogonal array with only two factors which are capacitance and gap voltage. Taguchi's L9 (3^2) orthogonal array was used to analyze the results and shown in Table 3.6. The total number of experiments in the set is 9. As well, the experiments were performed on both casted and 3D printed titanium alloys. Experiments for MRR and kerf width were performed on a 20 mm height surface towards inside the workpiece and measured when traveling 150 µm distance inside the material (on the right side of the plate according to Figure 3.6). For measuring hardness, crater size, surface roughness and contact angle, machining was done along the surface of the workpiece with 800 µm length (cuts on the middle of the plate according to Figure 3.6).

Figure 3.6: Top view on titanium plate for micro wire EDM

Table 3.6: Taguchi's orthogonal array for micro wire EDM

#	Capacitance, pF	Gap Voltage, V
1	1	90
2	1	100
3	1	110
4	10	90
5	10	100
6	10	110
7	100	90
8	100	100
9	100	110

For analysis of bacterial attachment and biofilm formation, several separate experiments were conducted on micro wire EDM with three different levels of discharge energy. Two 3 mm x 20 mm cuts were done, as shown in Figure 3.7, on the surface of 3D printed and casted alloys under low (1 pF and 90 V), medium (10 pF and 100 V) and high (100 pF and 110 V) discharge energy.

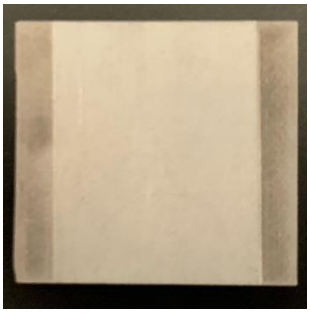

Figure 3.7: Top view on titanium plate for micro wire EDM

Regarding the parameters of machining, the material of wire electrode was tungsten carbide with diameter of 50 μm, wire speed and wire tension were constant and at 20% and 10% of machine capacity, respectively. EDM oil of hydrocarbon was used as dielectric fluid. Lastly, the feed rate of wire was set to 0.16 mm/min as the most optimal.

3.5. Post Experimental Analysis Procedure

After all surface treatments were done, post-experimental measurements and analysis were performed. Before gathering the data, plates are firstly cleaned in ultrasonic cleaner. After that, microscopic observations allowed to estimate MRR, overcut, kerf width and crater size from machined areas and scanning electron microscopy (SEM) photos. Also, surface roughness (SR), hardness and contact angle were measured as well for micro EDM treatment. Lastly, the tests on bacteria response were carried out.

3.5.1. Ultrasonic cleaner

After machining workpieces, they are cleaned by using ultrasonic cleaner in 95% ethanol liquid for 10-15 minutes. Then, the materials are rinsed with deionized water and dried with a dryer. This procedure allows the removal unnecessary debris that may affect further observations such as microscopic analyses, SEM photos, hardness tests and biological tests.

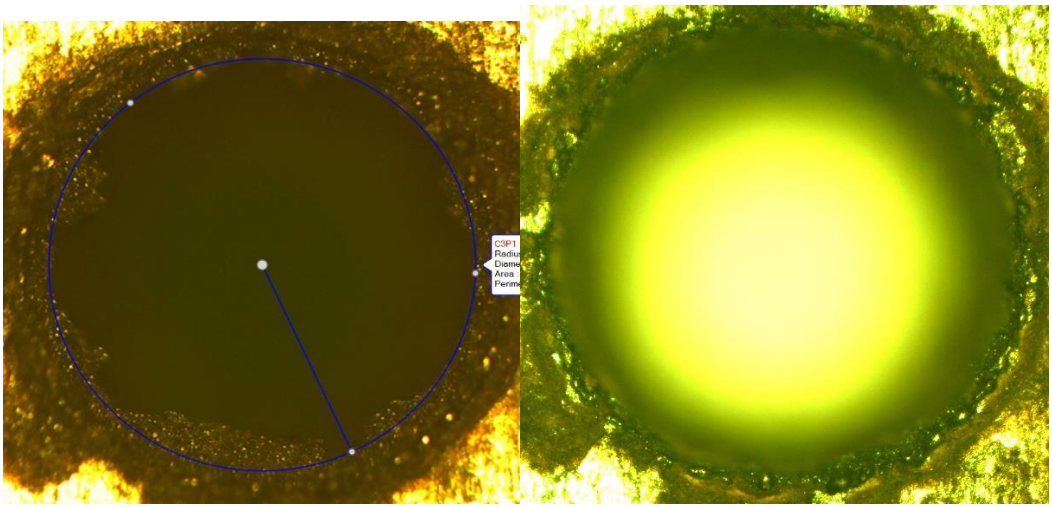

Figure 3.8: Microscopic photos of the same hole before (left) and after (right) ultrasonic cleaning.

As it is seen from the figure Figure 3.8, cleaning process is important in order to obtain precise results. The hole on the left side makes it difficult to estimate proper diameter due to the lack of detecting clean borders compared to the one on the right. Moreover, the total diameter of the clean hole is bigger because the debris stuck on the walls reducing visual ability to estimate the base of the material.

3.5.2. Microscopic analyses

After the workpieces were cleaned from debris, the visual representations of the holes were observed from microscope by using "Motic Images Plus 3.1." software. The measurements taken from microscopic observations allowed to estimate the dimensions of cuts machined by both drilling and micro EDM (see Figure 3.9), which, in turn, allowed to estimate MRR, OC and kerf width. For drilling EDM, these parameters can be calculated with the following equation:

$$MRR = \frac{Material\ removed}{Machining\ time} \quad (5)$$

$$OC = \frac{hole\ diameter\ at\ entrance - electrode\ diameter}{2}, \quad (6)$$

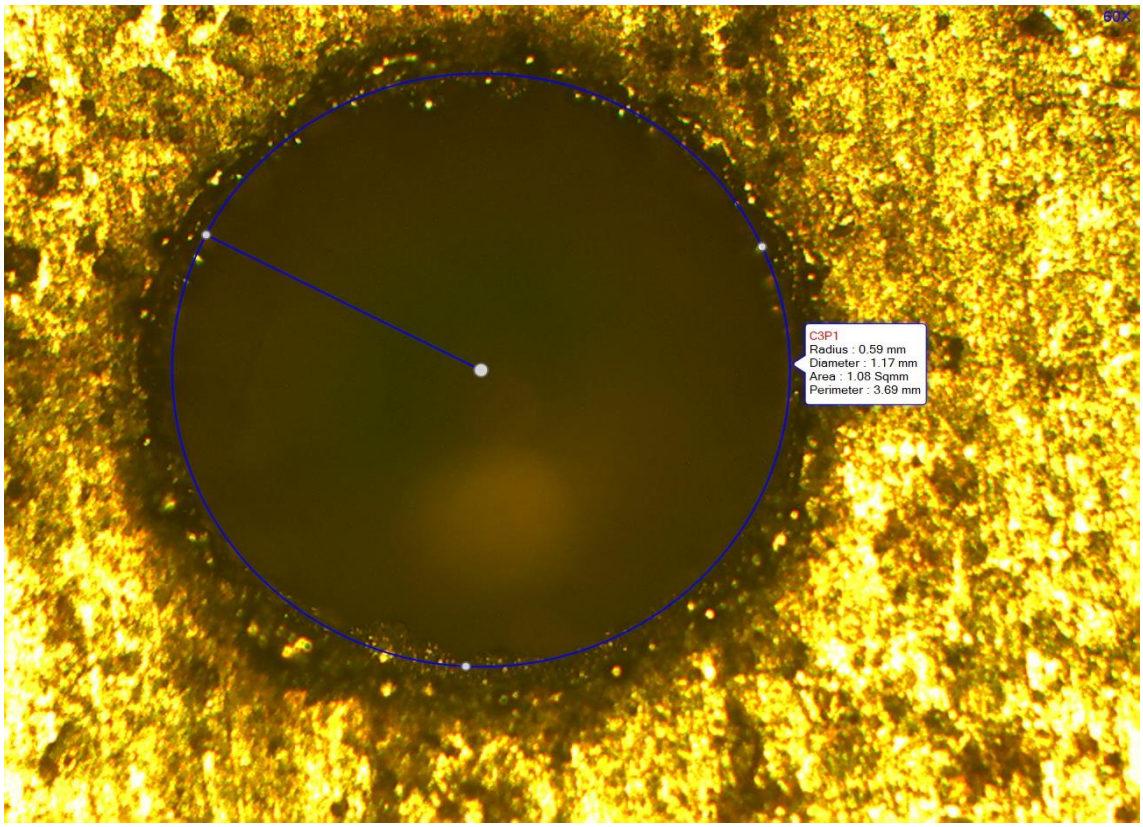

Figure 3.9: Measurements of hole diameter obtained from microscope for drilling EDM

Moreover, OC can be determined as the difference between hole diameter and electrode tool diameter. Lastly, wire cuts into the material allow to observe kerf width. By measuring kerf width at entrance and exit, MRR was calculated as well.

3.5.3. Scanning electron microscope (SEM)

By using SEM, the more precise images of the machined surfaces can be obtained as shown in Figure 3.10. This allows access to the newly formed surfaces. Moreover, it can estimate the chemical composition of surfaces, allowing to observe the contribution of tool electrodes on the surface composition, as shown in Figure 3.11 and Figure 3.12. The pictures obtained from SEM also provide quality images with high magnification allowing to precisely calculate crate size. In detail, the crater size was calculated by using ImageJ software (see Figure 3.13). By estimating the area of the crater, the average diameter was then calculated for average five measurements.

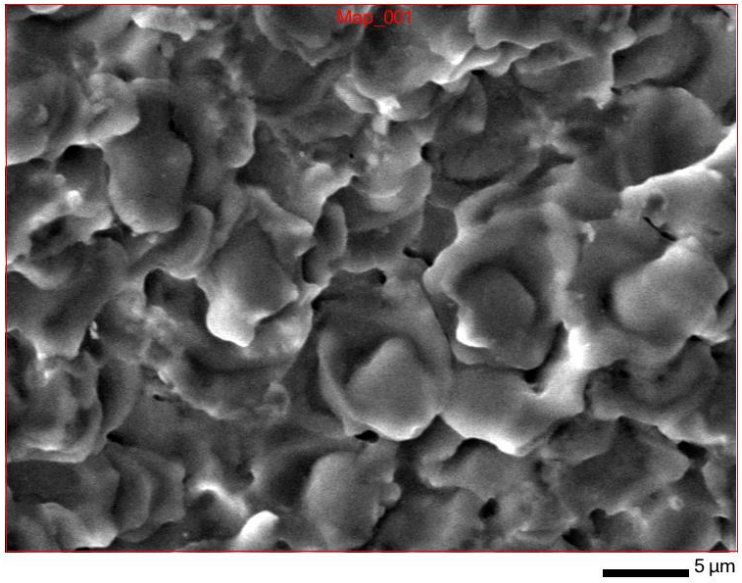

Figure 3.10: SEM photo of machined surface by micro wire EDM

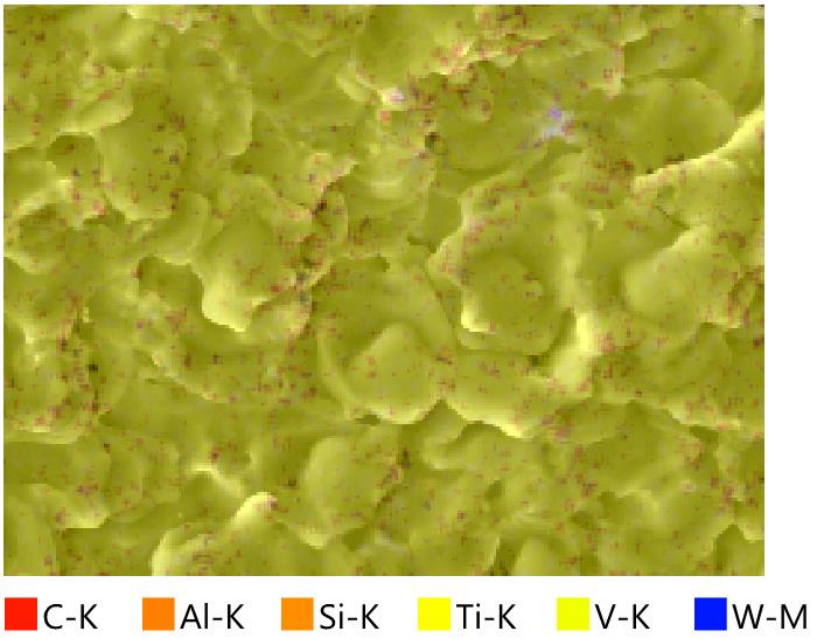

Figure 3.11: EDX analysis with SEM of a blind hole machined by micro EDM machine

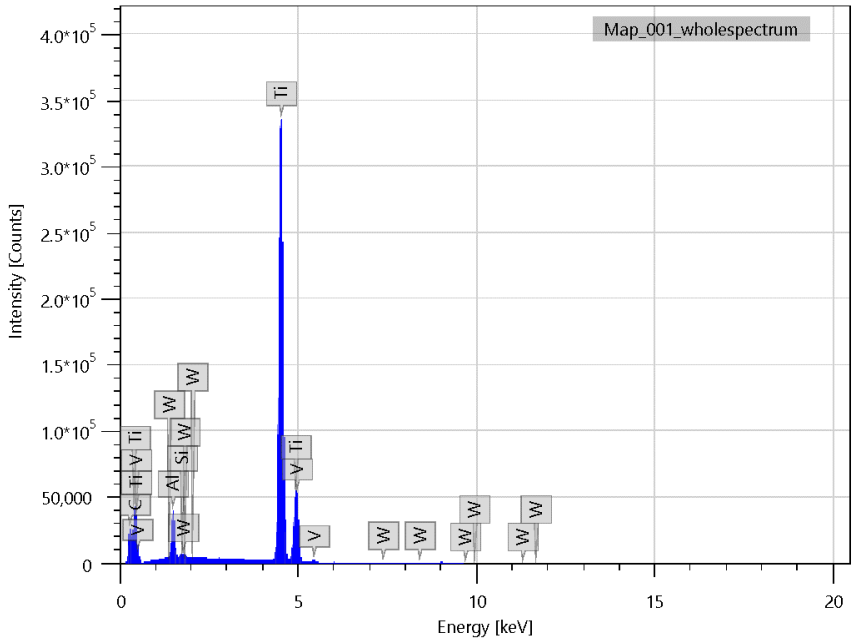

Figure 3.12: EDX analysis on elemental intensity obtained by SEM for a blind hole machined by micro EDM machine

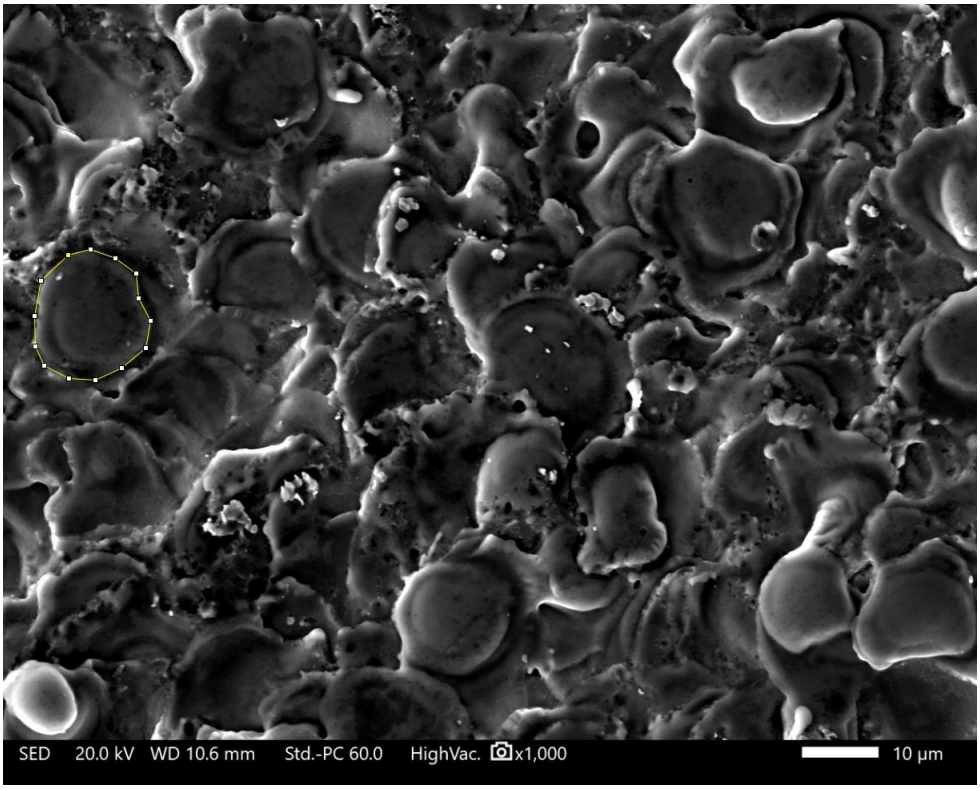

Figure 3.13: An example of measuring crater area with ImageJ software.

3.5.4. Hardness test

Hardness tester is able to observe the changes in mechanical properties of machined surfaces. The changes in microstructure after electro discharge treatment affect the hardness of the surfaces. FALCON 500 hardness testing tool investigates hardness in micro and macro scales. Vickers hardness test can be conducted on the sample surfaces. However, having 136^{o} degrees between two opposite faces the depth of the tests are limited. According to [19], the thickness of the recast layer varies between 2-5 μm in micro scale. In order to investigate changes in hardness in the proper way, the depth of indentation should not be more than the thickness of the recast layer. By considering the ratio of diagonal to depth which is approximately equal to 7:1, the diagonals for Vickers hardness test should be 30-20 μm which can be done under 200 g load for Ti-6Al-4V. Therefore, hardness tests were measured under 200 g load and 10 s of idle time for each machined surface. The measurements were taken five times and the average results were calculated accordingly for each alloy type.

3.5.5. Surface roughness

Surface roughness was measured with R-4000 by Hitechcn Enterprises Inc on wire machined surfaces. It has 90° conical tip with 5 μm radius mode of natural diamond. Each measurement was made for 0.8 mm length along the machined surface and repeated three times on different locations. The role of surface roughness is one of the important factors for successful cell adhesion. In fact, several experiments resulted in increased biocompatibility of treated surfaces. In tandem, the risk for bacteria adhesion and biofilm formation rises as well. By examining the capacity of the surface to prevent these issues, the criteria for Taguchi analysis were “smaller-is-better” (SB)

3.5.6. Contact angle

One of the parameters that affects bacteria adhesion to the surface is wettability of the surface. It can be measured with sessile drop test which estimates contact angle of three-phase contact between titanium surface, dielectric water and air. By using OCA 25 from DataPhysicsach experiment was done three times in order to estimate the average values of contact angles. From practical observations, many authors state that contact angle of the machined surfaces takes some part in successful integration of implants. It was observed that hydrophilic surfaces (which contact

angle is less than 90°) have better chances of cell adhesion. Despite that, as for human body cells, it is also increasing the chances of bacteria adhesion [20]. Since the following paper is focused more on the prevention of biofilm formation and bacteria attachment, the analysis of Taguchi's design was set as "larger-is-better" (LB).

3.5.7. Biological response

The biological aspects are also an important data to investigate. One of the aims of the work is to obtain results on biocompatibility of different treated surfaces. After machining and cleaning samples, the workpieces were tested for bacteria adhesion and biofilm formation. The strains of Pseudomonas Aeruginosa were used to measure the biofilm formation on various metal surfaces after 48 h of inoculation in broth culture. An initial optical density (OD600) of 0.1 or McFarland turbidity of 0.5 was used to create an inoculum from a fresh 24 h liquid culture of a single bacterial species to prepare the bacteria for culture. To calculate the volume of bacteria from 24 h culture, the standard formula C_1V_1 was used, where C_1, C_2 are the initial and final values of OD and V_1, V_2- initial and final volumes. Calculated number of bacteria was then added to the falcon with fresh media of volume 50 mL to obtain the final volume with an OD of 0.1. Each piece of metal was then submerged to a culture with a single species of bacteria in each falcon of volume 50 mL. The tubes were placed into a shaker incubator with a speed 220 RPM with temperature of 37°C for 48 hours. To identify the presence of bacterial cells and biofilm formation on the metal surfaces, the samples underwent staining with crystal violet dye. This was accomplished by immersing them in a crystal violet solution for a period of 30 minutes. To prepare samples for images, they were rinsed 3 times with distilled water and were left to dry at room temperature for 1 hour. Zeiss AxioZoom V16 macroscope was used to observe and image samples. Both brightfield and red fluorescent emission filter images were taken, with exposure times of 20 ms and 400 ms, respectively. A MatLab program was used for quantification of biofilm coverage. Additionally, before the biofilm formation test, the metals were placed under UV light for 30 minutes to ensure sterilization. It should be noted that P. aeruginosa was cultured in Luria-Bertani (LB) broth.

Chapter 4 –Optimization of EDM parameters

4.1. Introduction

This chapter shows the results obtained from the experimental studies and conducts discussion on them. Firstly, the results for macro EDM technique were presented in section 4.2. Then, these results were compared with the results for micro drilling EDM as well as more extensive analysis of the results from machining by micro wire EDM were discussed in chapter 4.3. Lastly, section 4.4 extends the discussion with correlations of each result between each other and their effect on biological results as well as the comparison between casted and SLM printer titanium alloys.

4.2. Drilling EDM results

The results from drilling EDM are shown in this section. The analysis on MRR and overcut with ANOVA technique as well as optimization of parameters for machining with multiple outputs by implementing grey relation analysis (GRA) were done in this section.

4.2.1. Material Removal Rate

The experimental results of MRR and its signal-to-noise (S/N) ratio are shown in Table 4.1, while Table 4.2 shows the ANOVA results with contribution weights for each of the machining parameters on MRR. It can be observed that pulse current is the most significant parameter that affects MRR with a 45.55% contribution, followed by the time-on parameter with a 33.56% contribution. The increased trends in S/N ratios as well as the increasing values for these two parameters shown in Figure 4.1 result in higher amounts of discharge energy, which affect MRR accordingly. The reason is that an increase in pulse current leads to an increase in discharge energy, while an increased time-on value lengthens the duration of each discharge pulse.

Table 4.1: Results of MRR and S/N ratios

Ex. No.	Control factor				MRR (10^{-1} mm^3/s)			S/N ratio
	I_p/ I_w	T_{on}	T_{off}	V_g	T1	T2	T3	
1	2	2	2	2	3.18	4.05	2.69	-9.61
2	2	5	5	5	3.01	3.55	3.29	-9.67
3	2	8	8	8	2.73	4.40	2.79	-9.61
4	5	2	5	8	3.27	4.11	3.36	-8.92
5	5	5	8	2	4.73	4.68	4.92	-6.42
6	5	8	2	5	6.19	7.13	5.55	-4.03
7	8	2	8	5	3.39	4.24	3.28	-8.79
8	8	5	2	8	5.52	6.23	5.17	-4.97
9	8	8	5	2	5.27	6.55	5.49	-4.78

Table 4.2: Results of ANOVA for MRR

Factor	Level 1	Level 2	Level 3	Sum of squares	DOF	Variance	Contribution %
Pulse current	-9.63	-6.45	-6.18	0.055	2	0.0274	45.55
Time-on	-9.11	-7.02	-6.14	0.040	2	0.0202	33.56
Time-off	-6.20	-7.79	-8.27	0.022	2	0.0111	18.47
Gap voltage	-6.94	-7.50	-7.83	0.003	2	0.0015	2.42
Error					0		
Total				0.120	8		100

From Figure 4.1, it can be observed that MRR increases at higher values of pulse current and time-on values and lower values of time-off and gap voltage. Despite that, the higher variances of the mean values of the S/N ratios of pulse current and time-on have a bigger impact compared to other parameters. By setting "larger-is-better" criteria for Taguchi's orthogonal array, the most optimal machining conditions for MRR can be obtained at A3B3C1D1. In order to verify its improvement in performance, the conformity test was done. The most optimal machining conditions for MRR in an orthogonal array were achieved in the 9th experiment which is A3B3C2D1. The average value of MRR is equal to 0.577 mm^3/s. Meanwhile, by using regression equation (7) for A3B3C1D1, the predicted value of MRR is equal to 0.664 mm^3/s which is 15% higher.

Regression equation for MRR:

$$\begin{aligned} MRR = {} & \mathbf{0,4399} - \mathbf{0.1100}\,A1 + \mathbf{0.04838}\,A2 + \mathbf{0.06162}\,A3 - \mathbf{0.08906}\,B1 \\ & + \mathbf{0.01676}\,B2 + \mathbf{0.07230}\,B3 + \mathbf{0.06799}\,C1 - \mathbf{0.01877}\,C2 \\ & - \mathbf{0.04922}\,C3 + \mathbf{0.02179}\,D1 + \mathbf{0.000423}\,D2 - \mathbf{0.02221}\,D3 \end{aligned} \quad (7)$$

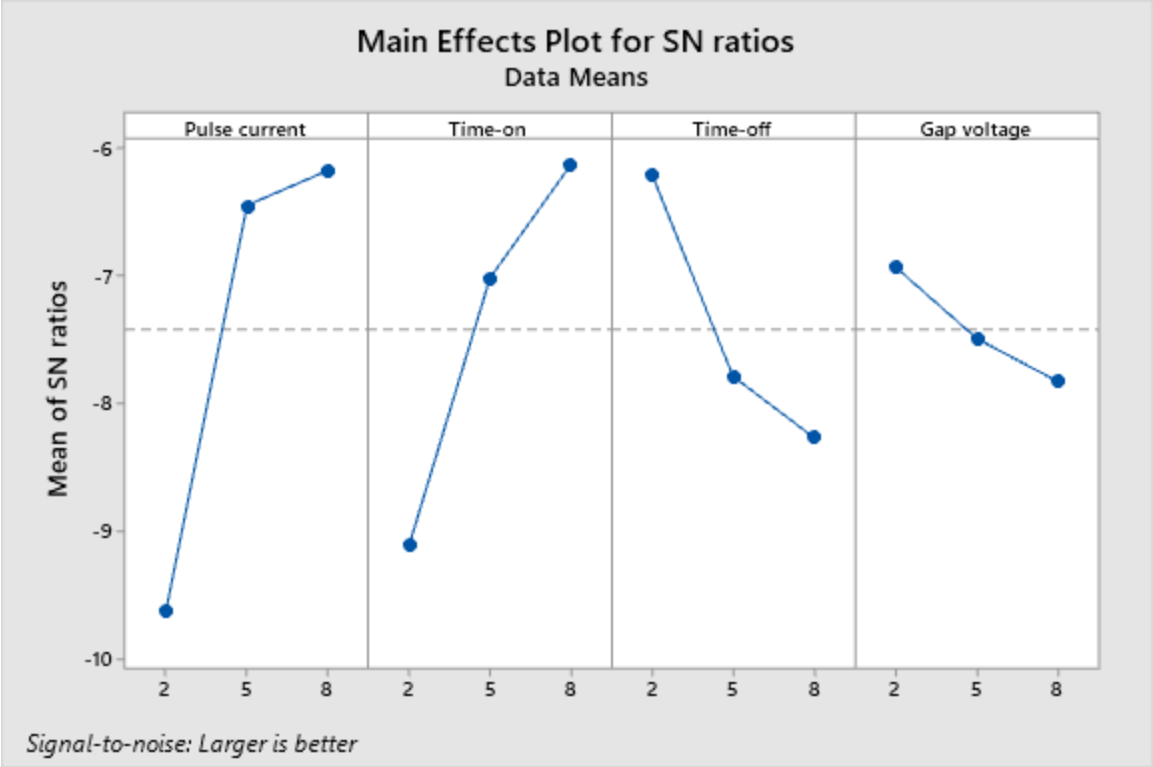

Figure 4.1: S/N response for MRR

4.2.2. Overcut

The results for overcut and its S/N ratios based on an orthogonal array are shown in Table 4.3. Also, results for ANOVA are listed in Table 4.4. The contribution of overcut is dominantly affected by time-on and time-off with 47.66% and 45.69%, respectively. In comparison, pulse current and gap voltage have little effect on overcut. The S/N ratio shows that the smaller time-on and time-off values result in a small overcut, which is possibly due to the higher frequency of pulses, which prevents concentration of discharge energy on a single point.

Table 4.3: Results of overcut and S/N ratio

Ex. No.	Control factor				Overcut (10^{-2} mm)			S/N ratio
	I_p/ I_w	T_{on}	T_{off}	V_g	T1	T2	T3	
1	2	2	2	2	5.75	6.26	5.64	24.6
2	2	5	5	5	6.81	7.09	7.09	23.1
3	2	8	8	8	7.58	6.74	7.98	22.6
4	5	2	5	8	6.16	5.86	6.31	24.3
5	5	5	8	2	6.86	6.83	7.34	23.1
6	5	8	2	5	6.16	6.90	6.70	23.6
7	8	2	8	5	6.96	6.63	6.20	23.6
8	8	5	2	8	5.53	6.20	6.13	24.5
9	8	8	5	2	6.75	8.30	7.14	22.6

Table 4.4: Results of ANOVA for overcut

Factor	Level 1	Level 2	Level 3	Sum of squares, $*10^{-4}$	DOF	Variance, $*10^{-4}$	Contribution %
Pulse current	23.4	23.7	23.6	0.06	2	0.03	2.19
Time-on	24.2	23.6	22.9	1.33	2	0.66	47.66
Time-off	24.2	23.3	23.1	1.27	2	0.64	45.69
Gap voltage	23.4	23.4	23.8	0.12	2	0.06	4.46
Error	$6.66*10^{-2}$				0		
Total	$1.15*10^{-6}$	$0.86*10^{-6}$	$0.02*10^{-6}$	2.78	8		100

Taguchi's analysis was performed with "smaller-is-better" criteria for overcut. According to Figure 4.2, the smallest overcut can be achieved at parameter settings of A2B1C1D3. By referring to the regression equation (6), the overcut under these conditions is expected to be equal to 54.2 μm. The smallest value of overcut obtained from experiments, referring to S/N ratios, is equal to 58.8 μm. The optimized conditions reduced overcut by 7.9%.

Regression equation for overcut:

$$\begin{aligned} \boldsymbol{Overcut} = {} & \mathbf{0.06662} + \mathbf{0,001074}\,\boldsymbol{A1} - \mathbf{0.000926}\,\boldsymbol{A2} - \mathbf{0.000148}\,\boldsymbol{A3} - \mathbf{0.004648}\,\boldsymbol{B1} \\ & - \mathbf{0.000107}\,\boldsymbol{B2} + \mathbf{0.004755}\,\boldsymbol{B3} - \mathbf{0.005218}\,\boldsymbol{C1} + \mathbf{0.001727}\,\boldsymbol{C2} \\ & + \mathbf{0.003491}\,\boldsymbol{C3} + \mathbf{0.001004}\,\boldsymbol{D1} + \mathbf{0.000643}\,\boldsymbol{D2} - \mathbf{0.001648}\,\boldsymbol{D3} \end{aligned} \quad (8)$$

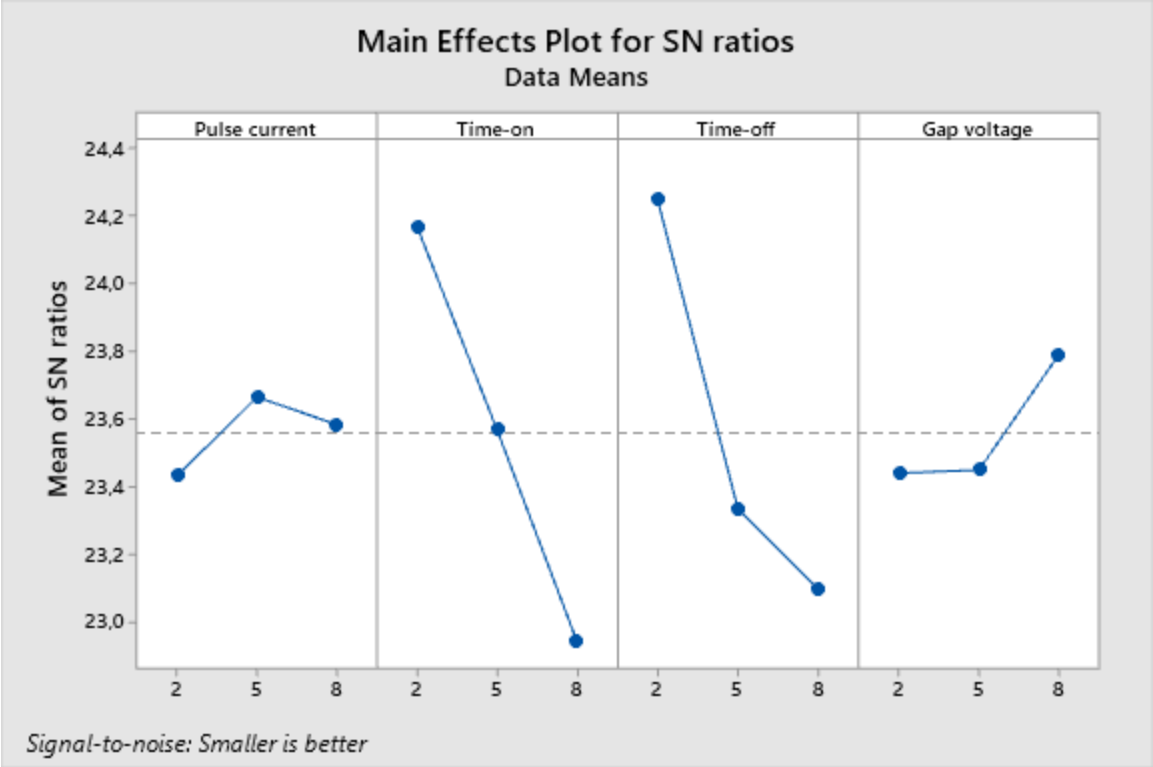

Figure 4.2: S/N response for overcut

4.2.3. Optimal EDM parameters

In order to analyze and estimate optimal machining parameters considering multiple types of results, grey relation analysis (GRA) is used. This technique is performed in several steps. First, normalization of each output dataset is done according to the "large-is-better" (LB) and "smaller-is-better" (SB) criteria. For the data with LB criteria, the values are normalized by the following formula:

$$y_i^*(k) = \frac{y(k) - \min y_i(k)}{\max y_i(k) - \min y_i(k)}, \tag{9}$$

Whereas normalization with SB criteria is estimated by the following formula:

$$y_i^*(k) = \frac{\max y_i(k) - y(k)}{\max y_i(k) - \min y_i(k)}. \tag{10}$$

There, i is the experiment number, k is the data sample number, $y_i(k)$ is the measurement value of the experiment i of data sample k, $\max y_i(k)$ and $\min y_i(k)$ are their maximum and minimum values. Second, the deviation sequence is calculated from the following equation:

$$\Delta_{0i}(\boldsymbol{k}) = \|\boldsymbol{y}_0^*(\boldsymbol{k}) - \boldsymbol{y}_i^*(\boldsymbol{k})\|. \quad (11)$$

Third, grey relation coefficients (GRC) are calculated by using the following formula:

$$\boldsymbol{\zeta}_i(\boldsymbol{k}) = \frac{\Delta_{min} + \boldsymbol{\zeta}.\Delta_{max}}{\Delta_{oi}(\boldsymbol{k}) + \boldsymbol{\zeta}.\Delta_{max}}, \quad (12)$$

Where ζ is the identification coefficient, which, for this study, was set to 0.5, Δ_{max} and Δ_{min} are the maximum and minimum values of $\Delta_{0i}(k)$. Lastly, grey relation grade (GRG) was obtained by taking the average value of GRC for each experiment number:

$$\boldsymbol{g}_i = \frac{\mathbf{1}}{\boldsymbol{n}}\sum_{\boldsymbol{k=1}}^{\boldsymbol{n}} \boldsymbol{\zeta}_i(\boldsymbol{k}). \quad (13)$$

By using equations (9-13), the GRG for each experiment was calculated and shown in Table 4.5. According to that, experiment 9 has the biggest GRG compared to the other nine experiments. As a result, machining parameters with $A_3B_3C_2D_1$ is the most optimal condition for experiment. The mean S/N ratios of GRG for each experiment are shown in Table 4.6. By referring to this table, the most optimal parameter set, based on GRA, is $A_3B_3C_2D_1$ which is experiment 9.

Table 4.5: Grey relation coefficient

No. Exp.	Grey relation coefficient		Grade
	MRR	Overcut	
1	0.336	0.333	0.335
2	0.333	0.660	0.497
3	0.336	1.000	0.668
4	0.366	0.374	0.370
5	0.541	0.667	0.604
6	1.000	0.492	0.746
7	0.372	0.495	0.434
8	0.749	0.344	0.547
9	0.790	0.963	0.876

Table 4.6: S/N response for GRG

Level	Pulse current	Time-on	Time-off	Gap voltage
1	0.500	0.380	0.543	0.605
2	0.573	0.549	0.581	0.559
3	0.619	0.764	0.569	0.528
Delta	0.119	0.384	0.039	0.077
Rank	2	1	4	3
Optimal	0.619	0.764	0.581	0.605

Meanwhile, Table 4.7 shows the results of GRA based on ANOVA. It demonstrates that time-on has a significant influence on multiple characteristics and performance, accounting for 87.08% of the contribution.

Table 4.7: ANOVA estimation for GRG

Factor	Level 1	Level 2	Level 3	DOF	Sum of squares	Variance	Contribution, %
Pulse current	0.500	0.574	0.619	2	0.022	0.011	8.51
Time-on	0.380	0.549	0.764	2	0.222	0.111	87.08
Time-off	0.542	0.581	0.569	2	0.002	0.001	0.91
Gap voltage	0.605	0.559	0.529	2	0.009	0.004	3.51
Error				0			
Total				8	0.255		

4.3. Micro EDM

The measurements of both micro drilling EDM and micro wire EDM are described in the current section. MRR, overcut and kerf width of both techniques as well as hardness, crater size, SR, contact angle and bacteria adhesion of wire treated surfaces are described below.

4.3.1. Material Removal Rate

The average experimental results from micro EDM drilling and their signal-to-noise (S/N) ratios are shown in Table 4.8. Also, the ANOVA calculations are illustrated in Table 4.9. According to the S/N ratios of each experiment, experiment number three has the highest performance on MRR, while experiment number five is the least effective one equal to $5.57*10^{-2}$ mm^3/s and $1.67*10^{-2}$ mm^3/s, respectively. The contribution weight of 86.86% depicts the major influence of capacitance value on MRR. Gap voltage affects only 11.07% while spindle speed of electrode almost has no effect having 1.67% of contribution. Figure 4.3, shows the mean values of S/N ratios.

Table 4.8: Results of MRR and S/N rations for micro drilling EDM on casted alloy

Exp. No.	Control factor			MRR (10^{-2} mm^3/s)	S/N ratio
	Voltage (V)	Capacitance (pF)	Spindle speed (rpm)		
1	90	1	750	4.11	-27,7
2	90	10	1000	1.76	-35,1
3	90	100	1250	5.57	-25,1
4	100	1	1000	4.66	-26,6
5	100	10	1250	1.67	-35,5
6	100	100	750	4.44	-27,1
7	110	1	1250	4.43	-27,1
8	110	10	750	1.82	-34,8
9	110	100	1000	5.42	-25,3

Table 4.9: Results of ANOVA for MRR from micro drilling EDM on casted alloy

Factor	Level 1	Level 2	Level 3	Sum of squares, $*10^{-3}$	DOF	Variance, $*10^{-3}$	Contribution %
Gap Voltage	-29.3	-29.7	-29.1	1.99	2	0.14	11.07
Capacitance	-27.1	-35.1	-25.8	15.64	2	7.52	86.86
Spindle Speed	-29.9	-29.0	-29.2	0.30	2	0.15	1.67
Error				0.07	2	0.04	0.40
Total				18.00	8		100

Comparing capacitance value of 1 pF and 100 pF, a slight increase in MRR is observable in Figure 4.3 due to the increase of discharge energy, however, at 10 pF capacitance MRR is decreased drastically which is the resulted from decrease of feed rate from feedback system. This system is triggered due to the debris generation misleadingly triggering the system to pull back an extra amount of path. Voltage has the same performance as capacitance but with less amplitude due to the less contribution. Spindle speed has an increasing average trend. Higher rotation speed allows to improve debris removal increasing MRR, however, excessive rotation is responsible for causing turbulent flow which decreases the capacity of flushing flow to remove debris. Estimating optimal MRR parameters, the experiment According to Figure 4.3 the most optimal combination of parameters for higher MRR is A3B3C2. By using regression equation below, the value of MRR for these parameters is equal to $5.41*10^{-2}$ mm^3/s.

The regression equation for MRR of micro drilling EDM on casted alloy:

$$\begin{aligned} MRR = {} & \mathbf{0.03672 + 0.00114\,A1 - 0.00378\,A2 + 0.00264\,A3 + 0.00467\,B1} \\ & \mathbf{- 0.01942\,B2 + 0.01476\,B3 - 0.00281\,C1 - 0.00006\,C2} \\ & \mathbf{+ 0.00287\,C3} \end{aligned} \quad (14)$$

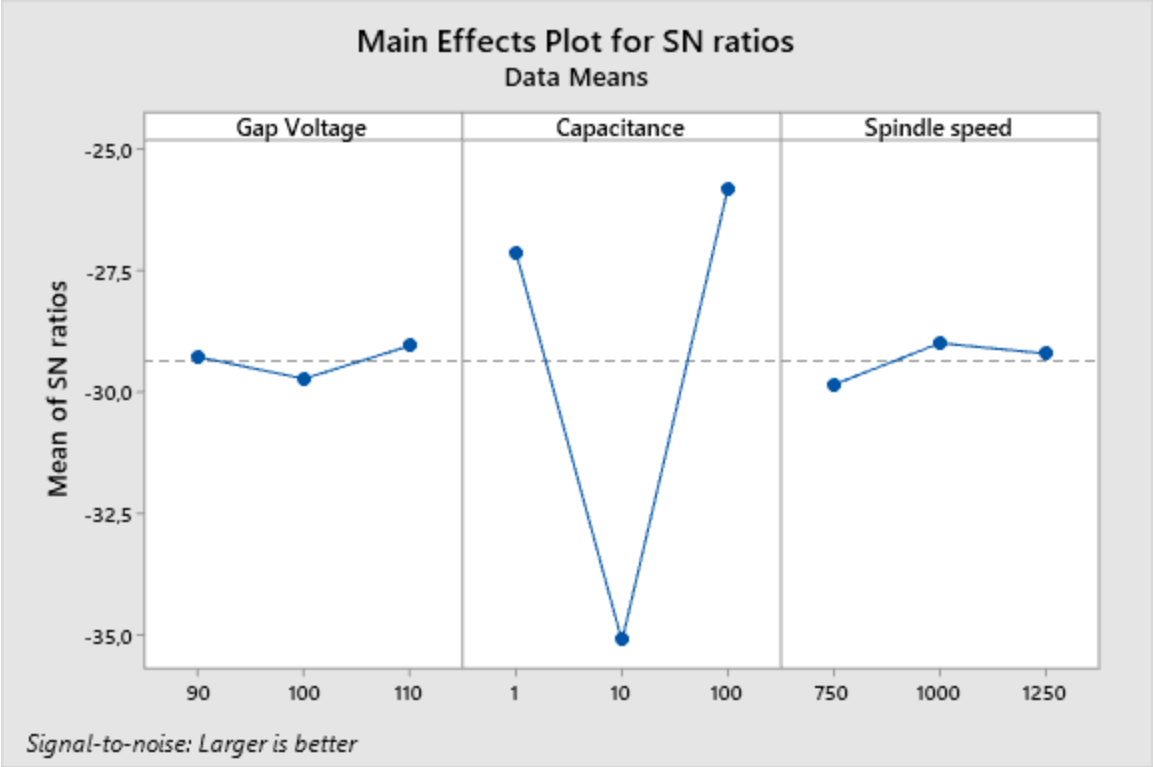

Figure 4.3: S/N response for MRR by micro drilling EDM on casted alloy

In addition to the results obtained from micro drilling EDM, the results of MRR for micro wire EDM were measured as well. Table 4.10 shows the obtained results of MRR and their signal-to-noise ratios for each experimental parameter. By comparing the S/N ratio of the experiments, the lowest highest performance is achieved at 1st level of capacitor and 3rd level of voltage while highest values of MRR is achieved at 2nd level of capacitance and 1st level of gap voltage. The contribution of both parameters shows that capacitor value has a bigger effect on MRR with 69.68% of weight. Meanwhile, less amount of contribution, which is 1.97%, is observed for gap voltage. The error value of 28.35% can be addressed to the other factors such as flushing conditions. Having an important value on removal of material, flushing flow rate was not able to be estimated, thus it was excluded from analysis.

In comparison, MRR of 3D printed titanium alloy was investigated. Table 4.10 shows the values of MRR and S/N ratios. Table 4.12 shows ANOVA observation based on the results. According to the S/N ratio, parameters set with highest discharge energy have the highest performance of MRR which is experiment number 9. Moreover, the contribution of capacitance over gap voltage is comparingly high, hiving 46.00% over 4.02% respectively. There is also a

reasonable value of error which is 49.98%. This can be referred to as the effect of flushing flow which is one of the major influences on the performance.

Table 4.10: Results of MRR and S/N rations for micro wire EDM on casted and printed alloys

Exp. No.	Control factor		Casted		Printed	
	Capacitance (pF)	Voltage (V)	MRR (10^{-2} mm^3/s)	S/N ratio	MRR (10^{-2} mm^3/s)	S/N ratio
1	1	90	1.34	-37.4	1.35	-37.4
2	1	100	1.21	-38.4	1.28	-37.9
3	1	110	1.13	-38.9	1.11	-39.1
4	10	90	1.72	-35.3	1.74	-35.2
5	10	100	1.60	-35.9	1.23	-38.2
6	10	110	1.48	-36.6	1.47	-36.7
7	100	90	1.17	-38.7	1.39	-37.2
8	100	100	1.40	-37.1	1.67	-35.5
9	100	110	1.44	-36.8	1.95	-34.2

Table 4.11: Results of ANOVA for MRR from micro wire EDM on casted alloy

Factor	Level 1	Level 2	Level 3	Sum of squares, $*10^{-3}$	DOF	Variance, $*10^{-3}$	Contribution %
Capacitance	-38.2	-35.9	-37.5	0.022	2	0.011	69.68
Gap Voltage	-37.1	-37.1	-37.5	0.001	2	0.000	1.97
Error				0.009	4	0.002	28.35
Total					8		100

Table 4.12: Results of ANOVA for MRR from micro wire EDM on printed alloy

Factor	Level 1	Level 2	Level 3	Sum of squares, $*10^{-3}$	DOF	Variance, $*10^{-3}$	Contribution %
Capacitance	-38.1	-36.7	-35.6	0.027	2	0.013	46.00
Gap Voltage	-36.6	-37.2	-36.7	0.002	2	0.001	4.02
Error				0.029	4	0.007	49.98
Total					8		100

Regression equation for MRR of micro wire EDM on casted alloy:

$$MRR = 0.013883 - 0.001611A1 + 0.002132A2 - 0.000522A3 + 0.000226B1 + 0.000145B2 + 0.000371B3 \quad (15)$$

Regression equation for MRR of micro wire EDM on printed alloy:

$$MRR = 0.014648 - 0.00218A1 + 0.00012A2 + 0.00205A3 + 0.00026B1 - 0.00071B2 + 0.00045B3 \quad (16)$$

From Figure 4.4, it is seen that the trendline of S/N ratios for capacitance is increasing with increase in its value resulting in proportional relation between MRR and capacitance value. However, the effect on gap voltage is the same as it was observed for micro drilling EDM.

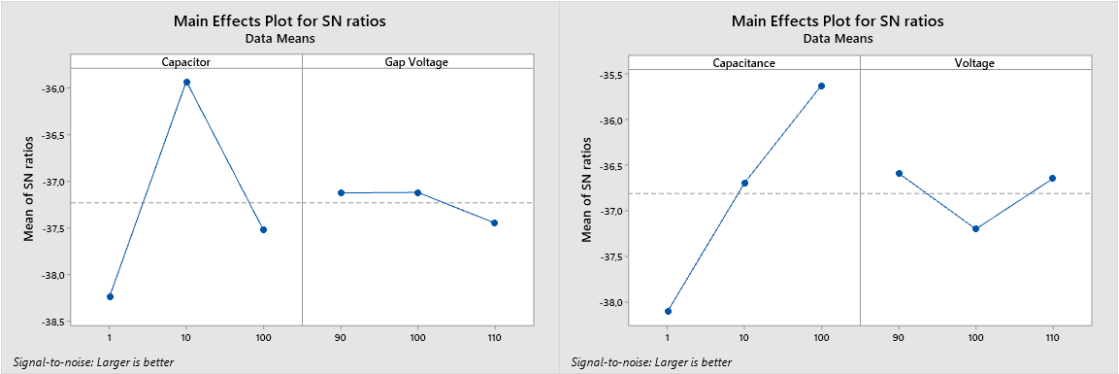

Figure 4.4: S/N response for MRR by micro wire EDM on casted alloy (left) and printed (right)

4.3.2. Overcut and Kerf width

The results of overcut for each experiment is shown in Table 4.13. As well, S/N ratio was calculated and shown. ANOVA results are represented in

Table 4.14. The value of overcut is almost completely dependent on capacitance value with 92.83% of contribution weight. For the rest, gap voltage and spindle speed contribute 3.48% and 1.43%, respectively. The remaining 2.26% is shared with external factors which had some effect on the experiment.

Table 4.13: Results of overcut and S/N rations for micro drilling EDM on casted alloy

Exp. No.	Control factor			Overcut (µm)	S/N ratio
	Voltage (V)	Capacitance (pF)	Spindle speed (rpm)		
1	90	1	750	2,08	-6,37
2	90	10	1000	9,10	-19,18
3	90	100	1250	15,11	-23,59
4	100	1	1000	0,43	7,38
5	100	10	1250	8,34	-18,42
6	100	100	750	12,91	-22,22
7	110	1	1250	2,65	-8,45
8	110	10	750	3,59	-11,10
9	110	100	1000	15,93	-24,04

Table 4.14: Result of ANOVA for overcut from micro drilling EDM on casted alloy

Factor	Level 1	Level 2	Level 3	Sum of squares	DOF	Variance	Contribution %
Gap Voltage	-16.38	-11.09	-14.53	0.45	2	0.07	3.48
Capacitance	-2.48	-16.23	-23.28	12.06	2	5.99	92.83
Spindle Speed	-13.23	-11.95	-16.82	0.19	2	0.09	1.43
Error				0.29	2	0.15	2.26
Total				12.99	8		100

According to Figure 4.5, capacitance performance is proportional. Having the most weight on overcut value, it provides less amount of overcut for less capacitance value and vice versa. However, gap voltage and spindle speed are slightly varying. Increase in spindle speed tends to decrease debris which could provide arcing increasing overcut. However, spindle speed at 1250 rpm can explain the presence of turbulence flow, which aborts the trend line. Gap voltage, also, results in smaller overcut from smaller discharge energy, but the same factor of debris removal has an effect on the results. Nevertheless, according to Figure 4.5, the most optimal parameters set can be achieved at A2B1C2 parameters. The regression formula for overcut estimated the value of 1.38 μm.

Regression equation for overcut of micro drilling EDM on casted alloy:

$$\boldsymbol{Overcut} = \mathbf{7.753 + 0.769\ A1 - 0.916\ A2 + 0.147\ A3 - 6.069\ B1 - 0.80\ B2 + 6.871\ B3 - 1.104\ C1 + 0.599\ C2 + 0.505\ C3} \quad (17)$$

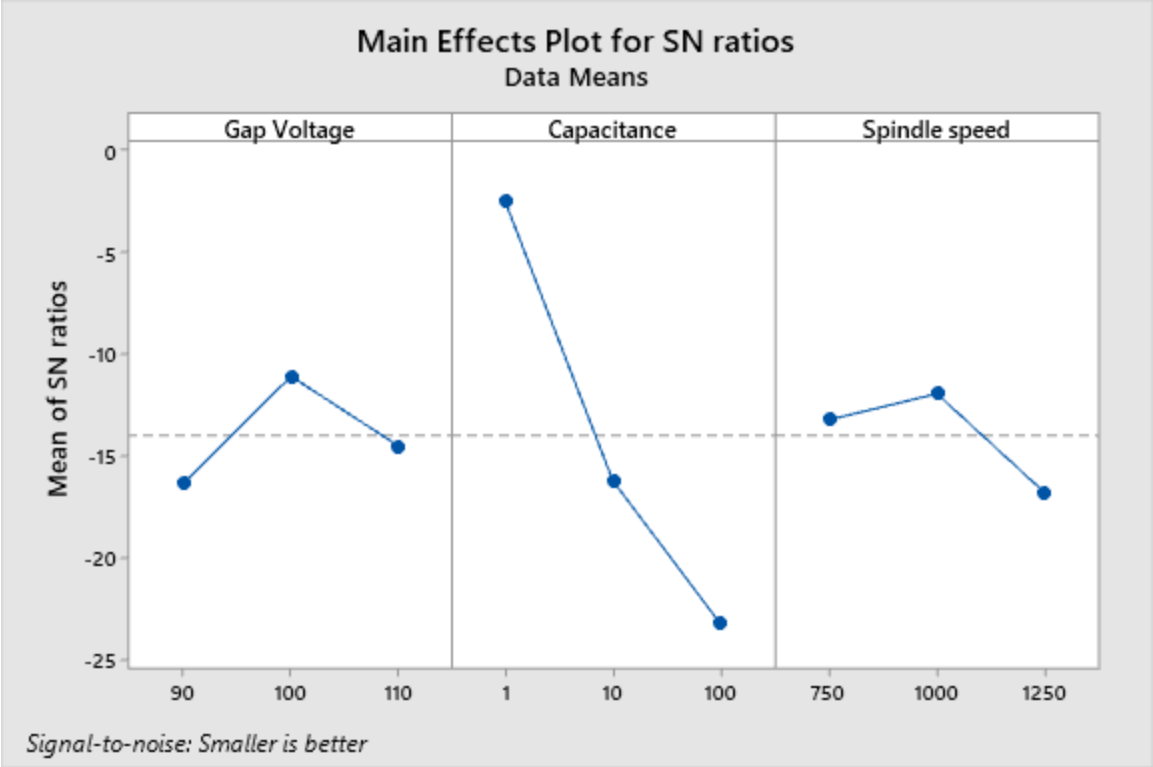

Figure 4.5: S/N response for overcut by micro drilling EDM on casted alloy

As for micro wire EDM, kerf width results for casted titanium alloys are shown in tables below. The average results of kerf width for each experiment are shown in Table 4.15. From analysis of S/N ratio, the small discharge energy results in less kerf width while 3rd level capacitance and 2nd level of gap voltage resulted in highest kerf width. From ANOVA, in Table 4.16, kerf width varies depending on capacitance and gap voltage with 69.68% and 1.97% contribution. A moderate error value is caused from high variance of kerf width on high discharge energy due to increased roughness of the surface. Moreover, local debris on high MRR value can lead to additional increase in spark distance due to the increase of electrical conductivity of the gap between tool and electrode.

Analyzing kerf width for 3D printed titanium alloy, its value varies accordingly to the change in discharge energy. The experimental observation from S/N ratios shows that the highest and lowest values of kerf width are obtained at 1st and 9th experiments which values are equal to 95.0 µm and 120.8 µm, respectively. Among that, the contribution of capacitance is higher than gap voltage which are 82.48% and 11.14%, respectively.

Table 4.15: Results of kerf width and S/N rations for micro wire EDM on casted and printed alloys

Exp. No.	Control factor		Casted		Printed	
	Capacitance (pF)	Voltage (V)	Kerf width (µm)	S/N ratio	Kerf width (µm)	S/N ratio
1	1	90	96.1	-39.7	95.0	-39.6
2	1	100	100.1	-40.0	96.9	-39.7
3	1	110	104.9	-40.4	103.5	-40.3
4	10	90	111.4	-40.9	105.9	-40.5
5	10	100	113.2	-41.1	100.3	-40.0
6	10	110	106.0	-40.5	106.3	-40.5
7	100	90	110.2	-40.8	111.5	-40.9
8	100	100	116.5	-41.3	116.9	-41.4
9	100	110	110.5	-40.9	120.8	-41.6

Table 4.16: Results of ANOVA for kerf width from micro wire EDM on casted alloy

Factor	Level 1	Level 2	Level 3	Sum of squares	DOF	Variance	Contribution %
Capacitance	-40.0	-40.8	-41.0	245.7	2	122.9	72.74
Gap Voltage	-40.5	-40.8	-40.6	25.5	2	12.8	7.55
Error				66.6	4	16.6	19.71
Total					8		100

Table 4.17: Results of ANOVA for kerf width from micro wire EDM on printed alloy

Factor	Level 1	Level 2	Level 3	Sum of squares	DOF	Variance	Contribution %
Capacitance	-39.9	-40.4	-41.3	502.3	2	251.1	82.48
Gap Voltage	-40.3	-40.4	-40.8	67.9	2	33.9	11.14
Error				35.9	4	9.7	6.38
Total					8		100

Regression equation for kerf width of micro wire EDM on casted alloy:

$$\boldsymbol{Kert\ width = 107.65 - 7.28A1 + 2.56A2 + 4.72A3 - 1.74B1 + 2.28B2 - 0.54B3} \quad (18)$$

Regression equation for kerf width of micro wire EDM on printed alloy:

$$\boldsymbol{Kerf\ width = 106.35 - 7.87A1 - 2.17A2 + 10.04A3 - 2.22B1 - 1.65B2 + 3.87B3} \quad (19)$$

From Figure 4.6, it is seen that the trendline of S/N ratios for capacitance is increasing with increase in its value resulting in proportional relation between MRR and capacitance value. However, the effect on gap voltage is the same as it was observed for micro drilling EDM.

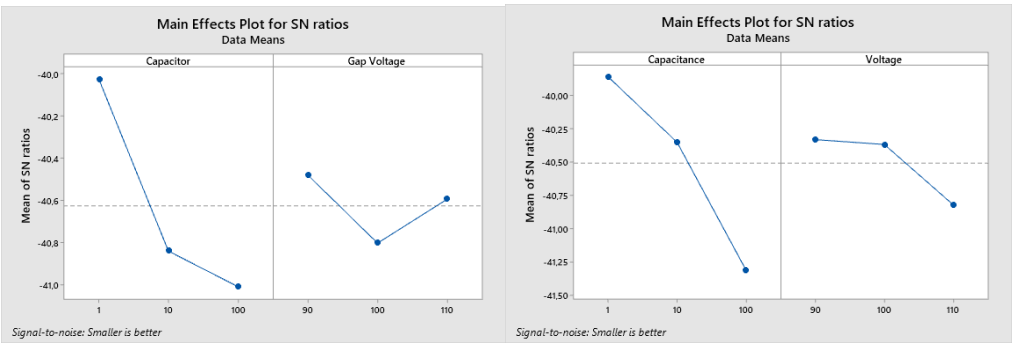

Figure 4.6: S/N response for kerf width by micro wire EDM on casted (left) and printed (right) alloy

4.3.3. Hardness

Performing hardness tests were suitable only for micro wire EDM on both casted and 3D printed titanium alloys. Hardness tests on modified surfaces of casted titanium alloy show that the smallest and highest values of hardness are equal to 335 HV and 528 HV on experiments 5 and 7 (see Table 4.18). From Table 4.19, the capacitance affects the hardness with 51.80% while gap voltage contributes 9.96%. The error values also take a reasonable place due to several factors such as a formation of tiny tungsten clusters, modified surface roughness, varying thickness of the recast layer and formation of porosity. Their presence can affect the hardness of the surface by both its increase or decrease. However, in order to avoid big misalignment of data, the measurements were taken based on 5 measurements with less deflection from the average value. Therefore, some of these factors can be avoided locally, but some of them are present inherent due to the nature of surface treatment technique.

Table 4.18: Results of hardness and S/N rations for micro wire EDM on casted and printed alloys

Exp. No.	Control factor		Casted		Printed	
	Capacitance (pF)	Voltage (V)	Hardness (HV)	S/N ratio	Hardness (HV)	S/N ratio
1	1	90	426	52.6	467	53.4
2	1	100	448	53.0	458	53.2
3	1	110	420	52.5	450	53.1
4	10	90	413	52.3	426	52.6
5	10	100	335	50.5	350	50.9
6	10	110	428	52.6	431	52.7
7	100	90	528	54.4	451	53.1
8	100	100	479	53.6	474	53.5
9	100	110	428	52.6	497	53.9

Table 4.19: Results of ANOVA for hardness from micro wire EDM on casted alloy

Factor	Level 1	Level 2	Level 3	Sum of squares, $*10^3$	DOF	Variance, $*10^3$	Contribution %
Capacitance	52.7	51.8	53.6	111.1	2	5.55	51.80
Gap Voltage	53.1	52.4	52.6	2.1	2	1.07	9.96
Error				8.2	4	2.05	38.24
Total					8		100

Table 4.20: Results of ANOVA for hardness from micro wire EDM on printed alloy

Factor	Level 1	Level 2	Level 3	Sum of squares	DOF	Variance	Contribution %
Capacitance	53.2	52.1	53.5	8550	2	4275	61.67
Gap Voltage	53.0	52.5	53.2	1552	2	776	11.19
Error				3763	4	941	27.14
Total					8		100

The hardness test conducted on 3D printed titanium alloy estimates almost similar overall performance as for casted titanium alloy. Table 4.18 shows the lowest and highest values of hardness are 350 HV and 497 HV. Despite the lowest value of hardness being observed during the same 5th experiment, the highest value of hardness obtained from the 9th experiment where the value of gap voltage changed from 1st level to 3rd level. Contribution of each factor also changed in a slight way. According to Table 4.20, the contribution of capacitance and gap voltage are equal to 61.67% and 11.19% respectively. As for the error, its value is equal to 27.14%.

Regression equation for hardness of micro wire EDM on casted alloy:

$$\boldsymbol{Hardness = 434.0 - 2.5A1 - 41.7A2 + 44.2A3 + 21.6B1 - 13.2B2 - 8.4B3} \quad (20)$$

Regression equation for hardness of micro wire EDM on printed alloy:

$$\boldsymbol{Hardness = 444.7 + 13.7A1 - 42.7A2 + 29.0A3 + 3.1B1 - 17.4B2 + 14.3B3} \quad (21)$$

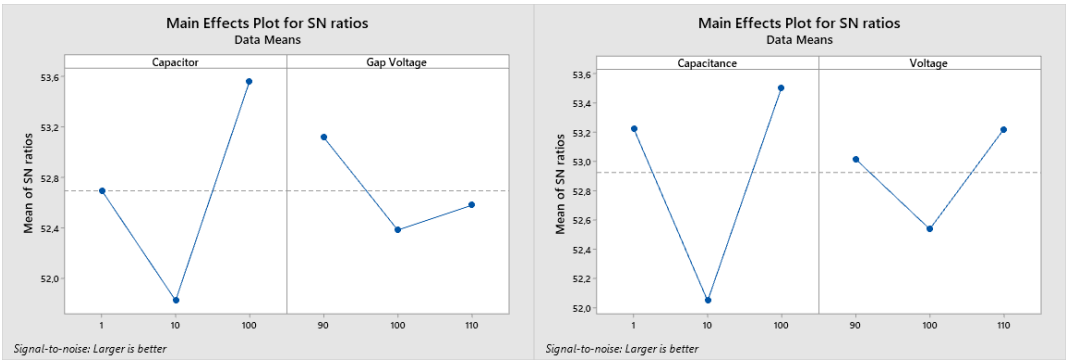

Figure 4.7: S/N response for hardness by micro wire EDM on casted alloy (left) and printed (right)

4.3.4. Crater size

The values of crater sizes for casted titanium alloy shows direct dependency on discharge energy in micro wire EDM. It can be observed from the values of crater diameters as well as their S/N ratios shown in Table 4.21. These results are mostly affected by capacitance value having weight of 93.53%, while effect from gap voltage is 5.10% (Table 4.22). The less amount of error states that there is a less effect by other not considered factors.

Crater sizes of 3D printed titanium alloy has the same performance with casted titanium alloy but with some minor differences. From the machining of both materials a slight reduction of crater sizes is observed for 3D printed alloy. The contribution of capacitance to the results increased from 93.53% to 95.32% while the contribution of gap voltage dropped from 5.10% to 2.60% (from Table 4.22 and Table 4.23).

Table 4.21: Results of crater size and S/N rations for micro wire EDM on casted and printed alloys

Exp. No.	Control factor		Casted		Printed	
	Capacitance (pF)	Voltage (V)	Crater size (µm)	S/N ratio	Crater size (µm)	S/N ratio
1	1	90	6.93	-16.8	5.82	-15.3
2	1	100	6.10	-15.7	5.81	-15.3
3	1	110	8.89	-19.0	6.81	-16.7
4	10	90	12.12	-21.7	12.16	-21.7
5	10	100	13.87	-22.8	13.01	-22.3
6	10	110	15.48	-23.8	13.56	-22.6
7	100	90	20.77	-26.4	19.78	-25.9
8	100	100	23.80	-27.5	24.62	-27.8
9	100	110	26.95	-28.6	25.87	-28.3

Table 4.22: Results of ANOVA for crater size from micro wire EDM on casted alloy

Factor	Level 1	Level 2	Level 3	Sum of squares	DOF	Variance	Contribution %
Capacitance	-17.2	-22.8	-27.5	416.18	2	208.09	93.53
Gap Voltage	-21.6	-22.0	-23.8	22.71	2	11.35	5.10
Error				6.08	4	1.52	1.37
Total					8		100

Table 4.23: Results of ANOVA for crater size from micro wire EDM on printed alloy

Factor	Level 1	Level 2	Level 3	Sum of squares	DOF	Variance	Contribution %
Capacitance	-15.7	-22.2	-27.3	455.11	2	227.56	95.32
Gap Voltage	-21.0	-21.8	-22.5	12.43	2	6.21	2.60
Error				9.90	4	2.47	2.07
Total					8		100

Regression equation for crater size of micro wire EDM on casted alloy:

$$\boldsymbol{Crater\ diameter} = \mathbf{14.990 - 7.685A1 - 1.165A2 + 8.850A3 - 1.713B1 - 0.401B2 + 2.115B3} \quad (22)$$

Regression equation for crater size of micro wire EDM on printed alloy:

$$\boldsymbol{Crater\ diameter} = \mathbf{14.160 - 8.017A1 - 1.249A2 + 9.267A3 - 1.572B1 + 0.319B2 + 1.253B3} \quad (23)$$

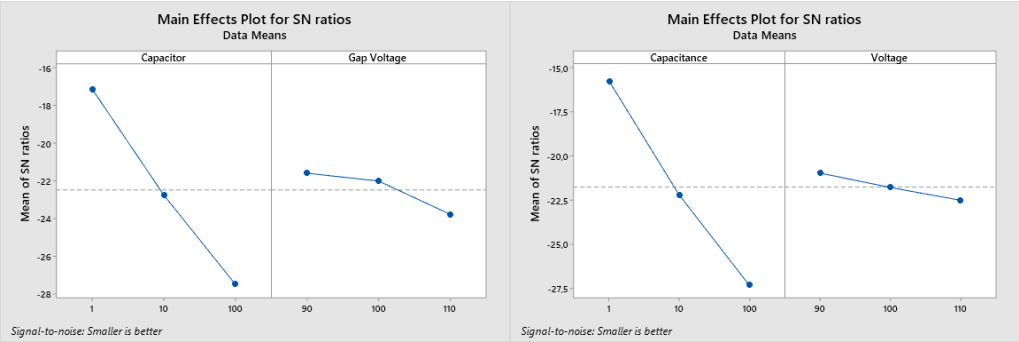

Figure 4.8: S/N response for crater size by micro wire EDM on casted alloy (left) and printed (right)

4.3.5. Surface roughness

The roughness values of treated surfaces were changed after EDM modification according to the values of the discharge energy. Drastic increases of surface roughness at different capacitance values result in significant effect on surface roughness (see Table 4.24) with

contribution of 99.33% and 92.48% for casted (Table 4.25) and printed (Table 4.26) alloy, respectively. In comparison, the effects of gap voltage for both materials are very small.

It can be observed from Table 4.24 that the surface roughness of printed alloy is consistently lower than that of the casted alloy for most experimental factors. This finding suggests that the surface finish of the 3D printed alloy is superior to the casted alloy, which can be attributed to the better control of the printing process resulting in more consistent and uniform microstructure.

Table 4.24: Results of surface roughness and S/N rations for micro wire EDM on casted and printed alloys

Exp. No.	Control factor		Casted		Printed	
	Capacitance (pF)	Voltage (V)	Surface roughness (µm)	S/N ratio	Surface roughness (µm)	S/N ratio
1	1	90	0.309	10.21	0.211	13.51
2	1	100	0.301	10.44	0.276	11.18
3	1	110	0.306	10.30	0.277	11.15
4	10	90	0.680	3.35	0.665	3.54
5	10	100	0.686	3.27	0.727	2.77
6	10	110	0.763	2.35	0.761	2.37
7	100	90	1.524	-3.66	1.893	-5.54
8	100	100	1.655	-4.37	1.253	-1.96
9	100	110	1.680	-4.51	1.531	-3.70

Table 4.25: Results of ANOVA for surface roughness from micro wire EDM on casted alloy

Factor	Level 1	Level 2	Level 3	Sum of squares	DOF	Variance	Contribution %
Capacitance	10.32	2.99	-4.18	2.71960	2	1.35980	99.33
Gap Voltage	3.30	3.11	2.71	0.00933	2	0.00467	0.34
Error				0.00904	4	0.00226	0.33
Total					8		100

Table 4.26: Results of ANOVA for surface roughness from micro wire EDM on printed alloy

Factor	Level 1	Level 2	Level 3	Sum of squares	DOF	Variance	Contribution %
Capacitance	11.95	2.90	-3.74	2.6245	0	1.3122	92.48
Gap Voltage	3.84	4.00	3.27	0.0445	0	0.0223	1.57
Error				0.1688	4	0.0422	5.95
Total					8		100

Regression equation for surface roughness of micro wire EDM on casted alloy:

$$\boldsymbol{Surface\ roughness} = \mathbf{0.8781} - \mathbf{0.5731}\boldsymbol{A1} - \mathbf{0.1683}\boldsymbol{A2} + \mathbf{0.7414}\boldsymbol{A3} - \mathbf{0.0406}\boldsymbol{B1} + \mathbf{0.0023}\boldsymbol{B2} + \mathbf{0.0382}\boldsymbol{B3} \quad (24)$$

Regression equation for surface roughness of micro wire EDM on printed alloy:

$$\boldsymbol{Surface\ roughness} = \mathbf{0.8439} - \mathbf{0.5892}\boldsymbol{A1} - \mathbf{0.1262}\boldsymbol{A2} + \mathbf{0.7154}\boldsymbol{A3} + \mathbf{0.0791}\boldsymbol{B1} - \mathbf{0.0917}\boldsymbol{B2} + \mathbf{0.0126}\boldsymbol{B3} \quad (25)$$

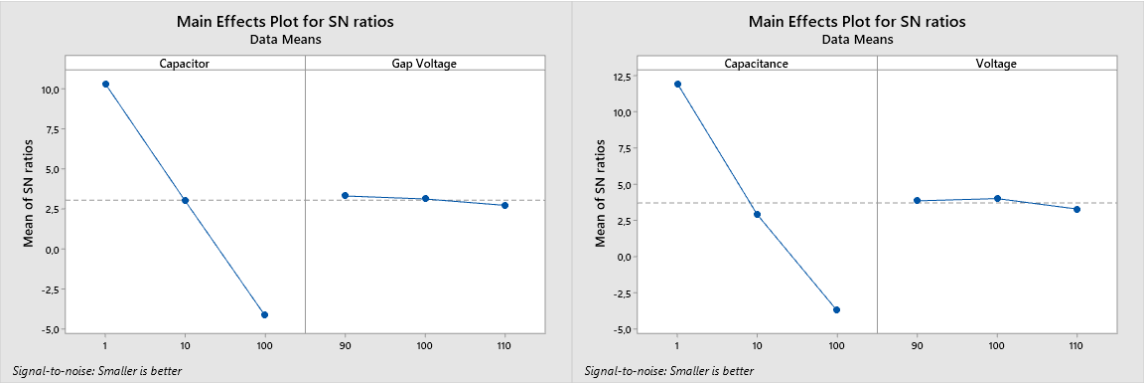

Figure 4.9: S/N response for surface roughness by micro wire EDM on casted alloy (left) and printed (right)

4.3.6. Contact angle

The results of the Taguchi analysis for wire electro discharge machining (EDM) on casted and printed Ti-6Al-4V alloys for contact angle are presented in Table 4.27, Table 4.28 and Table 4.29. The contact angle and S/N ratio were measured for both types of alloys, and the ANOVA was performed to analyze the contribution of each control factor on the contact angle.

Table 4.27 shows that the contact angle and S/N ratio vary depending on the control factors, capacitance and gap voltage, and the type of alloy, casted or printed. For casted alloys, the highest contact angle was observed at the capacitance of 110 pF and gap voltage of 90 V, whereas for printed alloys, the highest contact angle was observed at the capacitance of 100 pF and gap voltage of 110 V. The S/N ratio for both types of alloys was relatively similar, with the highest value being obtained for printed alloys at the capacitance of 10 pF and gap voltage of 110 V.

Table 4.27: Results of contact angle and S/N rations for micro wire EDM on casted and printed alloys

Exp. No.	Control factor		Casted		Printed	
	Capacitance (pF)	Voltage (V)	Contact angle (◦)	S/N ratio	Contact angle (◦)	S/N ratio
1	1	90	59.2	35.4	52.0	34.3
2	1	100	60.1	35.6	58.7	35.4
3	1	110	69.1	36.8	71.3	37.1
4	10	90	66.1	36.4	64.1	36.1
5	10	100	63.4	36.0	64.0	36.1
6	10	110	70.9	37.0	74.4	37.4
7	100	90	69.2	36.8	71.4	37.1
8	100	100	71.8	37.1	71.9	37.1
9	100	110	67.3	36.6	60.6	35.6

Table 4.28: Results of ANOVA for contact angle from micro wire EDM on casted alloy

Factor	Level 1	Level 2	Level 3	Sum of squares	DOF	Variance	Contribution %
Capacitance	35.9	36.5	36.8	67.9	2	33.9	40.57
Gap Voltage	36.2	36.3	36.8	34.5	2	17.2	20.60
Error				64.9	4	16.2	38.83
Total					8		100

Table 4.29: Results of ANOVA for contact angle from micro wire EDM on printed alloy

Factor	Level 1	Level 2	Level 3	Sum of squares	DOF	Variance	Contribution %
Capacitance	35.6	36.6	36.6	125.0	2	62.5	41.43
Gap Voltage	35.8	36.2	36.7	106.4	2	53.2	35.26
Error				70.3	4	17.6	23.31
Total					8		100

Table 4.28 and Table 4.29 present the results of ANOVA for contact angle for casted and printed alloys, respectively. In both cases, the capacitance and gap voltage factors were found to significantly contribute to the variance in contact angle. For casted alloys, the capacitance factor had a higher contribution percentage (40.57%) than the gap voltage factor (20.60%). In contrast, for printed alloys, the capacitance and gap voltage factors had similar contribution percentages (41.43% and 35.26%, respectively).

Regression equation for contact angle of micro wire EDM on casted alloy:

$$\boldsymbol{Contact\ angle = 66.35 - 3.57A1 + 0.46A2 + 3.11A3 - 1.51B1 - 1.25B2 + 2.76B3} \quad (26)$$

Regression equation for contact angle of micro wire EDM on printed alloy:

$$\boldsymbol{Contact\ angle = 65,37 - 4,71A1 + 2,13A2 + 2,58A3 - 2,89B1 - 0.51B2 + 3,39B3} \quad (27)$$

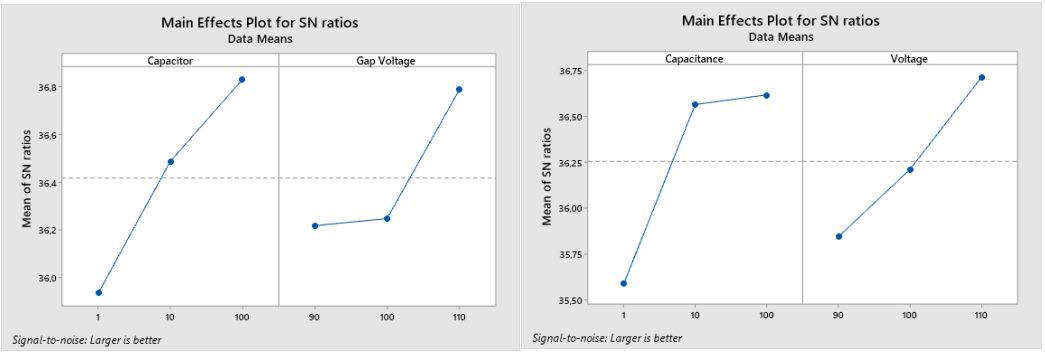

Figure 4.10: S/N response for contact angle by micro wire EDM on casted alloy (left) and printed (right)

4.3.7. Biological response

The test on the biofilm formation of the modified surfaces was done for Pseudomonas Aeruginosa. The overall performance on prevention of biofilm formation of Ti-6Al-4V alloy was noticeable. In fact, only few bacterial colonies were observed locally on machined surfaces. Firstly, tiny bacteria colonies were observed in several zones. The pictures used with crystal violet from Table 4.30 marks bacteria colonies with red color. It was discovered that for casted titanium alloys low discharge energy (1nF and 90 V) machining is more advantageous for bacteria adhesion and biofilm formation compered to high discharge energy (100nF and 110 V). However, for medium discharge energy (10 nF and 100 V), there were almost no bacteria strains on machined surfaces. Meanwhile, tests revealed that there are several small colonies on machined surfaces of printed titanium alloy. The presence of bacteria on capacitance 1 nF and gap voltage of 90 V is small but still higher than other machined surfaces. While there is a smaller number of bacteria on surfaces machined with 100 nF and 110 V, bacteria strains on surfaces machined with medium energy were not observed. Generally, the tendency of bacteria adhesion and biofilm formation on the Ti-6Al-4V alloy is low, however, it rises for machining surfaces with smaller discharge energies. Nevertheless, there are several bigger colonies on casted alloy while printed alloy inherited a small local strain.

Table 4.30: Results on biofilm formation of Pseudomonas Aeruginosa on treated surfaces

Casted	**Crystal violet (left side)**	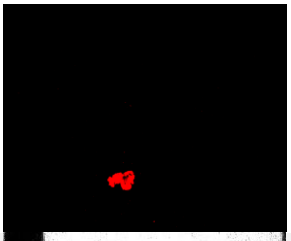		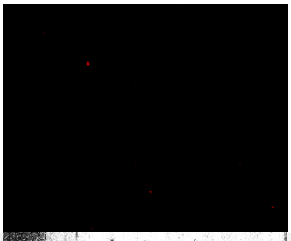
	Microscope (left side)			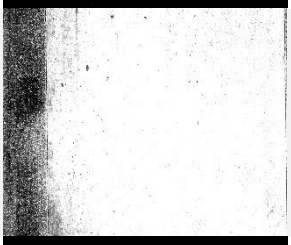
	Crystal violet (right side)			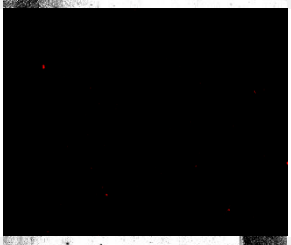
	Microscope (right side)		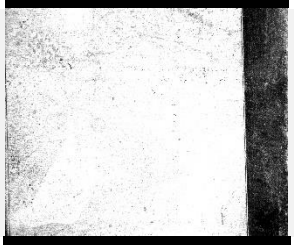	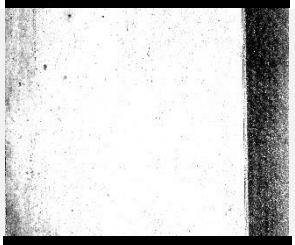
Printed	Crystal violet (left side)			
	Microscope (left side)		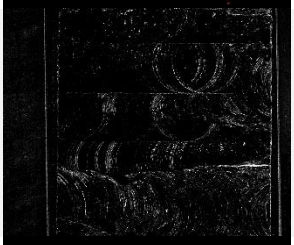	
	Crystal violet (right side)			

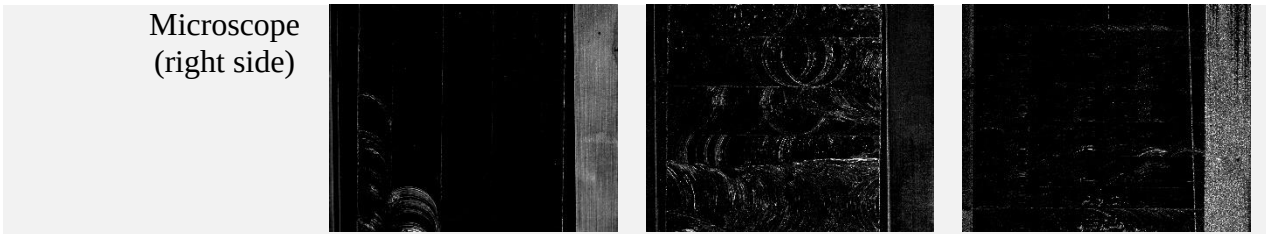

4.3.8. Optimal values of output parameters

By performing analysis of the above results, statistical analysis allows to estimate regression equations for each output parameter. Table 4.31 shows the most optimal inputs for these parameters and their predicted values. These results investigate the differences in EDM performance between the casted and printed alloys, and the optimal settings for the input parameters, which are capacitance and gap voltage.

The comparison between the casted and printed alloys showed that the optimal settings for the input parameters differ, indicating that the performance of the EDM process is influenced by the material characteristics. The SLM printed alloy had better optimized performance for MRR, kerf width, crate size and SR while casted alloy had better optimized performance for contact angle and hardness.

Table 4.31: Optimal values of output parameters according to S/N analysis

Output	**Signal-to-noise ratio**	**Casted**		**Printed**	
		Value	Input	Value	Input
MRR	LB	0.0162 mm^3/s	A2B1	0.0171 mm^3/s	A3B3
Kerf width	SB	98.6 µm	A1B1	96.3 µm	A1B1
Hardness	LB	500 HV	A3B1	488 HV	A3B3
Crater size	SB	5.59 µm	A1B1	4.57 µm	A1B1
SR	SB	0.264 µm	A1B1	0.163 µm	A1B2
Contact angle	LB	72.2°	A1B1	71.3°	A1B1

4.4. Correlation between the results.

The performance of EDM in terms of discharge energy showed that bigger sparks lead to larger amounts of material removed. Discharge energy mostly relies on capacitance values during

the micro EDM process. Although there are some deflections of the output parameters during micro drilling and wire EDM caused from the lack of debris removal, macro drilling EDM results validate that with increase of pulse current and time-on values the MRR increases. With the increase of discharge energy, the values of overcut and kerf width increase respectfully for micro drilling and wire EDM. There are direct correlations between overcut/kerf width, crate sizes and surface roughness can be observed. All of these parameters show that increase in discharge energy led to increase in overcut/kerf width, crate size and surface roughness in the same behavior.

Despite that, the results obtained from the hardness test have a different behavior under different machining energy. The average values of hardness predicted by ANOVA for the discharge energy of 4.05 μJ are equal to 453 HV and 462 HV for casted and printed titanium alloy. The hardness after machining with the highest discharge energy of 605 μJ is equal to 470 HV and 488 HV, respectively. However, during the medium energy of 50 μJ, the values of hardness were minimal for both casted and printed alloy and equal to 379 HV and 385 HV, respectively. By refereeing SEM images, different amounts of energy level can modify surface the with several differences in topography. Small material removal led to a more uniform surface, while big energy has an excessive amount of remelted material making the surface uniform in such a way. However, during medium machining energy several porous regions were observed. The hardness of the tested region is decreased due to the internal structure of the recast layer having porosity or metallic voids.

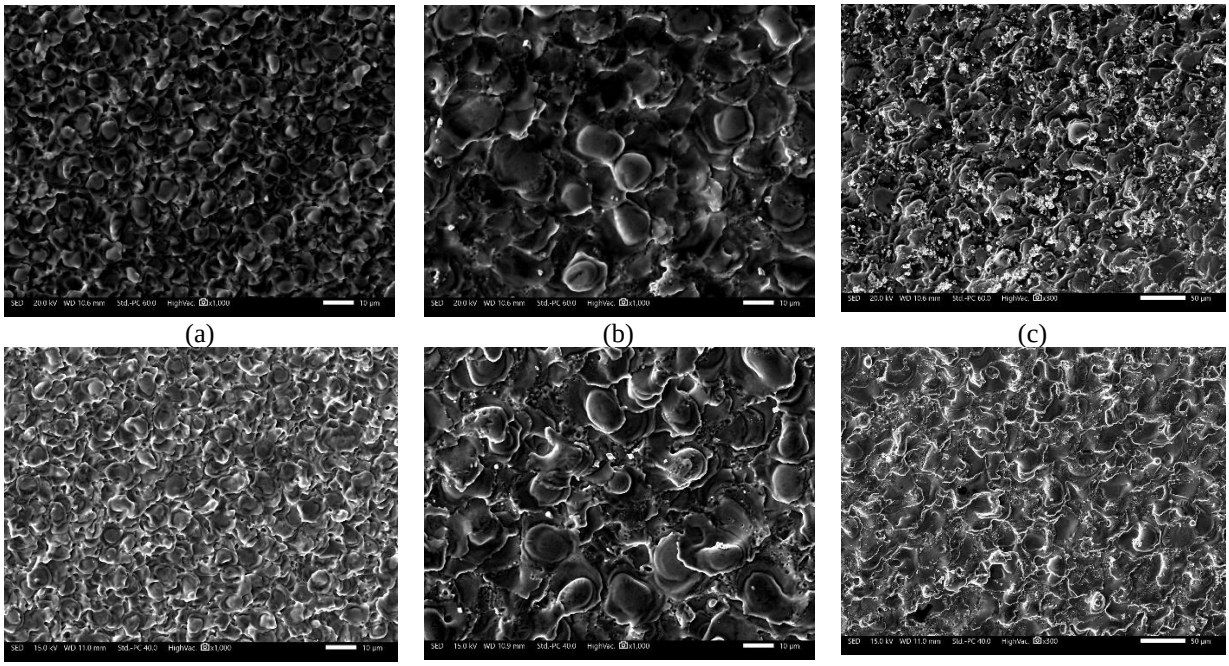

(a) (b) (c)

(d) (e) (f)

Figure 4.11: SEM images of machined surfaces of casted (a-c) and printed alloys where left, middle and right are machined with low, medium and high energy, respectively

Regarding the sessile drop tests, it was observed that wettability of the surfaces with low surface roughness and crater size values are better, compared to the results with their high values. Also, during the experiments, it was discovered that water propagation along the surface with high surface roughness was slower compared to less rough surfaces. This is caused from an increased contact area between rough surface and water leading to an increase in friction. For that reason, good wettability obtained from low discharge energy led to relatively more bacteria adhesion and biofilm formation of Pseudomonas Aeruginosa on Ti-6Al-4V.

According to the results between casted and printed titanium alloys, the performances of the most optimal parameters for printed titanium alloy are slightly overweight casted alloy in most parameters except microhardness. Even though, both Ti-6Al-4V plates show good biofilm prevention capacity, bacteria strain on printed titanium alloy is less compared to the casted alloy.

Chapter 5 – Conclusion and Future Work

5.1. Conclusion

In conclusion, the study of EDM surface treatment on biomedical Ti-6Al-4V alloy was done. By aiming to investigate the effects of this technique on improvement of biocompatibility aspects, several experiments were done with drilling EDM, micro drilling EDM and micro wire EDM. The effects of parameters of both micro and macro EDM machining such as gap voltage, working current, capacitance, time-on and time-off were observed by implementing Taguchi's orthogonal array and ANOVA. These results analyzed the performance of the EDM in terms of MRR, overcut, kerf width, SR, crate size, contact angle and hardness for different machining parameters. Moreover, biofilm formation and bacteria adhesion were investigated as well. Micro wire EDM was utilized as the main surface treatment technique. Nevertheless, some performance such as MRR and overcut were compared with micro drilling EDM which was in turn validated with macro drilling EDM. As a result, all of them produced analogous behavior. Moreover, the study was focused on investigating the difference between casted titanium alloy and 3D SLM printed titanium alloy. Finally, all of these procedures were performed in order to thoroughly correlate the contribution of EDM technique to biocompatibility of Ti-6Al-4V alloy.

During the experimental investigations there were several points concluded which are:

- Discharge energy directly affects the results of MRR, overcut/kerf width, crater size, surface roughness, and contact angle.
- Hardness of accessed regions can be both increased or decreased according to the amount of discharge energy.
- Biological investigations showed that smaller amounts of energy have a tendency to improve adhesion. It was observed that while machining titanium plates with micro wire EDM and energy of 4.05 μJ, the bacteria colonies were higher comparing to the observations from discharge energies of 50 μJ and 605 μJ
- Comparison between casted and printed titanium alloys shows that printed titanium alloy is more effective in most measured output results.

Finally, this paper shows that SLM has a good potential in printing biomedical implants having better results compared to casted titanium alloy. Moreover, it was investigated that higher discharge energy of EDM increases the resistance of bacteria adhesion and biofilm formation.

5.2. Contribution to Knowledge

This work focused on contributing knowledge in the field of material science as well as biomedicine. Considering the existence of several issues in the area of successful implant bone replacement, attempts of combination of several technologies as well as exploration of new directions of problem solution were contributed.

In fact, there are only a few studies of the combination of the SLM process of printing Ti-6Al-4V implant and its surface treatment with EDM technique. Moreover, the number of conducted studies on bacteria analysis of EDM treated Ti-6Al-4V is small. This thesis work contributes to the experimental studies in this research gap which needs more research.

5.3. Future Work

For future work, investigation of EDM techniques on improving biocompatibility of titanium alloy implants can be extended to more broad scope in terms of biological analysis such as evaluating body cell adhesion and wide variety of bacteria. Moreover, combination of SLM printed parts with EDM machined surfaces can be investigated in-depth for enhancing orthopedic application of implants.

References

[1] M. Kaur and K. Singh, "Review on titanium and titanium based alloys as biomaterials for orthopaedic applications," *Materials Science and Engineering: C,* vol. 102, pp. 844-862, 2019/09/01/ 2019.

[2] X. Liu, P. K. Chu, and C. Ding, "Surface modification of titanium, titanium alloys, and related materials for biomedical applications," *Materials Science and Engineering: R: Reports,* vol. 47, no. 3, pp. 49-121, 2004/12/24/ 2004.

[3] C. Prakash, H. K. Kansal, B. S. Pabla, S. Puri, and A. Aggarwal, "Electric discharge machining - A potential choice for surface modification of metallic implants for orthopedic applications: A review," *Proceedings of the Institution of Mechanical Engineers, Part B: Journal of Engineering Manufacture,* Review vol. 230, no. 2, pp. 331-353, 2016.

[4] M. S. Baltatu *et al.*, "Biocompatible titanium alloys used in medical applications," vol. 70, no. 4, pp. 1302-1306, 2019.

[5] A. T. Sidambe, "Biocompatibility of advanced manufactured titanium implants-A review," *Materials,* Review vol. 7, no. 12, pp. 8168-8188, 2014.

[6] B. W. Lai, Y. Y. Chang, T. M. Shieh, and H. L. Huang, "Biocompatibility and microstructure-based stress analyses of tinbzrta composite films," *Materials,* Article vol. 15, no. 1, 2022, Art. no. 29.

[7] G. Lazzini, L. Romoli, A. H. A. Lutey, and F. Fuso, "Modelling the interaction between bacterial cells and laser-textured surfaces," *Surface and Coatings Technology,* Article vol. 375, pp. 8-14, 2019.

[8] N. Eliaz, "Corrosion of Metallic Biomaterials: A Review," *Materials,* vol. 12, no. 3, 2019.

[9] G. Singh, T. R. Ablyaz, E. S. Shlykov, K. R. Muratov, A. S. Bhui, and S. S. Sidhu, "Enhancing Corrosion and Wear Resistance of Ti6Al4V Alloy Using CNTs Mixed Electro-Discharge Process," *Micromachines,* vol. 11, no. 9, 2020.

[10] K. H. Ho and S. T. Newman, "State of the art electrical discharge machining (EDM)," *International Journal of Machine Tools and Manufacture,* vol. 43, no. 13, pp. 1287-1300, 2003/10/01/ 2003.

[11] P. Harcuba, L. Bačáková, J. Stráský, M. Bačáková, K. Novotná, and M. Janeček, "Surface treatment by electric discharge machining of Ti–6Al–4V alloy for potential application in orthopaedics," *Journal of the Mechanical Behavior of Biomedical Materials,* vol. 7, pp. 96-105, 2012/03/01/ 2012.

[12] S. Saha, "Experimental Investigation of the Dry Electric Discharge Machining (Dry EDM) Process," 2008.

[13] M. Priyadarshini, C. Biswas, and A. Behera, "Machining of sub-cooled low carbon tool steel by wire-EDM," *Materials and Manufacturing Processes,* vol. 34, 09/09 2019.

[14] C. Y. Yap *et al.*, "Review of selective laser melting: Materials and applications," *Applied Physics Reviews,* Review vol. 2, no. 4, 2015, Art. no. 041101.

[15] H. Hassanin, F. Modica, M. A. El-Sayed, J. Liu, and K. Essa, "Manufacturing of Ti–6Al–4V Micro-Implantable Parts Using Hybrid Selective Laser Melting and Micro-Electrical Discharge Machining," *Advanced Engineering Materials,* Article vol. 18, no. 9, pp. 1544-1549, 2016.

[16] B. B. Pradhan, M. Masanta, B. R. Sarkar, and B. Bhattacharyya, "Investigation of electro-discharge micro-machining of titanium super alloy," *The International Journal of Advanced Manufacturing Technology,* vol. 41, no. 11, p. 1094, 2008/06/10 2008.

[17] W.-F. Lee, T.-S. Yang, Y.-C. Wu, P.-W. J. J. o. E. Peng, and C. Medicine, "Nanoporous biocompatible layer on Ti–6Al–4V alloys enhanced osteoblast-like cell response," vol. 5, no. 3, pp. 92-96, 2013.

[18] M. Jahan, F. Alavi, R. Kirwin, R. J. I. J. o. M. Mahbub, and M. o. Materials, "Micro-EDM induced surface modification of titanium alloy for biocompatibility," vol. 20, no. 3, pp. 274-298, 2018.

[19] M. P. Jahan, P. Kakavand, and F. Alavi, "A comparative study on micro-electro-discharge-machined surface characteristics of Ni-Ti and Ti-6Al-4V with respect to biocompatibility," *Procedia Manufacturing,* vol. 10, pp. 232-242, 2017.

[20] Q. Zheng, L. Mao, Y. Shi, W. Fu, and Y. J. M. T. Hu, "Biocompatibility of Ti-6Al-4V titanium alloy implants with laser microgrooved surfaces," vol. 37, no. 12, pp. 2039-2048, 2022.